Cell Reports

Article

Apyrase-mediated amplification of secretory IgA promotes intestinal homeostasis

Graphical abstract

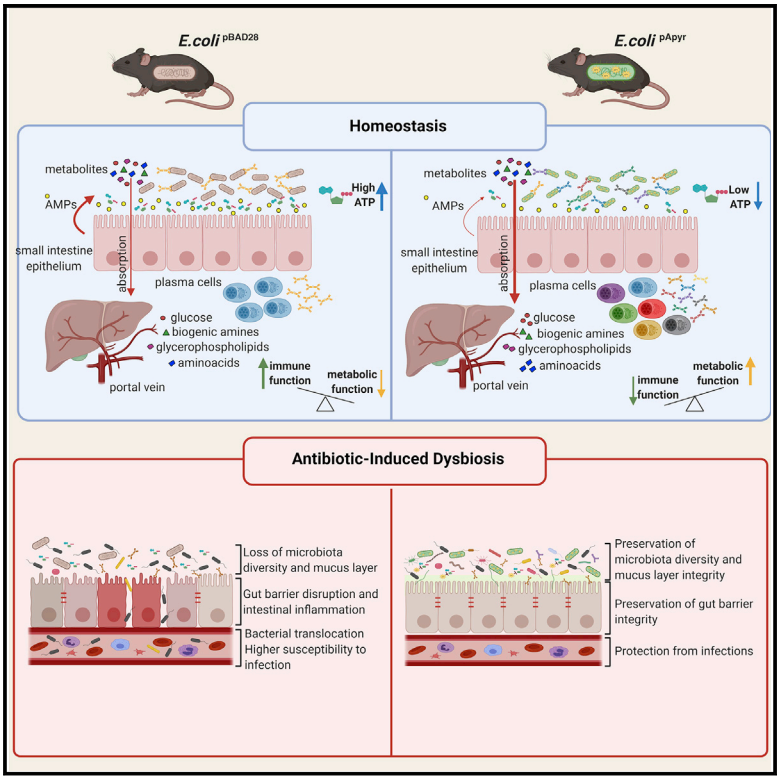

Highlights

- Extracellular ATP modulates the secretory IgA (SIgA) response in the intestine
- Delivery of the ATP-degrading enzyme apyrase amplifies the breadth of SIgA repertoire
- Enhanced SIgA coating of the microbiota by apyrase conditions enterocyte function
- Enhanced SIgA coating of the microbiota preserves gut integrity during dysbiosis

Authors

Lisa Perruzza, Francesco Strati, Matteo Raneri, ..., Simone Guglielmetti, Victor Greiff, Fabio Grassi

Correspondence

fabio.grassi@irb.usi.ch

In brief

Secretory IgA plays pleiotropic function in ensuring the integrity of the intestinal ecosystem. Perruzza et al. show that amplification of gut SIgA repertoire by hydrolysis of endoluminal extracellular ATP can condition enterocyte transcriptional activity and promote intestinal homeostasis and colonization resistance in dysbiosis.

Perruzza et al., 2022, Cell Reports *40*, 111112
July 19, 2022
https://doi.org/10.1016/j.celrep.2022.111112

CellPress

Cell Reports

CellPress
OPEN ACCESS

Article

Apyrase-mediated amplification of secretory IgA promotes intestinal homeostasis

Lisa Perruzza,[1,8] Francesco Strati,[1,7,8] Matteo Raneri,[1] Hai Li,[2] Giorgio Gargari,[3] Tanja Rezzonico-Jost,[1] Martina Palatella,[1] Ivo Kwee,[1] Diego Morone,[1] Frauke Seehusen,[4] Paolo Sonego,[5] Claudio Donati,[5] Pietro Franceschi,[5] Andrew J. Macpherson,[2] Simone Guglielmetti,[3] Victor Greiff,[6] and Fabio Grassi[1,9,*]

[1]Institute for Research in Biomedicine, Faculty of Biomedical Sciences, Università della Svizzera Italiana, Bellinzona 6500, Switzerland
[2]Maurice Müller Laboratories, Department of Biomedical Research, Universitätsklinik für Viszerale Chirurgie und Medizin, Inselspital, University of Bern, Bern 3010, Switzerland
[3]Division of Food Microbiology and Bioprocesses, Department of Food, Environmental and Nutritional Sciences (DeFENS), University of Milan, Milan 20133, Italy
[4]Institute of Veterinary Pathology, Vetsuisse Faculty, University of Zurich, Zurich 8057, Switzerland
[5]Unit of Computational Biology, Research and Innovation Centre, Fondazione Edmund Mach, San Michele all'Adige (TN) 38098, Italy
[6]Department of Immunology and Oslo University Hospital, University of Oslo, Oslo 0372, Norway
[7]Present address: Mucosal Immunology Lab, Department of Experimental Oncology, European Institute of Oncology (IEO), Milan, Italy
[8]These authors contributed equally
[9]Lead contact
*Correspondence: fabio.grassi@irb.usi.ch
https://doi.org/10.1016/j.celrep.2022.111112

SUMMARY

Secretory immunoglobulin A (SIgA) interaction with commensal bacteria conditions microbiota composition and function. However, mechanisms regulating reciprocal control of microbiota and SIgA are not defined. Bacteria-derived adenosine triphosphate (ATP) limits T follicular helper (Tfh) cells in the Peyer's patches (PPs) via P2X7 receptor (P2X7R) and thereby SIgA generation. Here we show that hydrolysis of extracellular ATP (eATP) by apyrase results in amplification of the SIgA repertoire. The enhanced breadth of SIgA in mice colonized with apyrase-releasing *Escherichia coli* influences topographical distribution of bacteria and expression of genes involved in metabolic versus immune functions in the intestinal epithelium. SIgA-mediated conditioning of bacteria and enterocyte function is reflected by differences in nutrient absorption in mice colonized with apyrase-expressing bacteria. Apyrase-induced SIgA improves intestinal homeostasis and attenuates barrier impairment and susceptibility to infection by enteric pathogens in antibiotic-induced dysbiosis. Therefore, amplification of SIgA by apyrase can be leveraged to restore intestinal fitness in dysbiotic conditions.

INTRODUCTION

The intestine ensures the digestion and absorption of nutrients and, concomitantly, the establishment and maintenance of a beneficial microbial community (Chow et al., 2011). The gut microbiota is essential for intestinal and immune system differentiation, tissues homeostasis, and systemic metabolism (Sommer and Backhed, 2013). Alterations in the microbial community structure have been associated to susceptibility to diseases (Blaser, 2006), and dysbiosis to an increasing number of medical conditions, including metabolic disorders (e.g., diabetes, obesity), blood pressure alteration, and autoimmunity (Cerf-Bensussan and Gaboriau-Routhiau, 2010; Dicksved et al., 2008; Holmes et al., 2008; Larsen et al., 2010; Scher et al., 2013; Turnbaugh et al., 2009; Wu et al., 2010). Many factors contribute to the shaping of the gut microbiota, but specific mechanisms responsible for host microbiota mutualism are not thoroughly understood.

The glycan-rich gut mucous layer constitutes an essential niche for symbionts by providing nutrients and a scaffold for growth (Backhed et al., 2005; Li et al., 2015). Secretory immunoglobulin A (SIgA) may enhance commensal colonization of this microbial niche by promoting adhesion and/or nutrient utilization of bacteria within the colonic mucus (Johansson et al., 2008; Rogier et al., 2014). In fact, immunoglobulin A (IgA)-coated bacteria contribute to host physiology and metabolism (Perruzza et al., 2019) and are important for the preservation of commensals diversity and community networks in the human gut (Fadlallah et al., 2018). Recently, a regulatory system where IgA fosters mucosal colonization of the human intestinal commensal *Bacteroides fragilis* was described (Donaldson et al., 2018; Lee et al., 2013). Furthermore, glycan-dependent, epitope-independent IgA coating of *Bacteroides thetaiotaomicron*, a prominent gut symbiont of the phylum Bacteroidetes, regulated gene transcription and metabolism by inducing the expression of polysaccharide utilization loci, which in turn promoted symbiosis with other members of the gut microbiota and colonic homeostasis (Nakajima et al., 2018).

Because the immune system and the gut microbiota start developing together at birth, it has been hypothesized that their

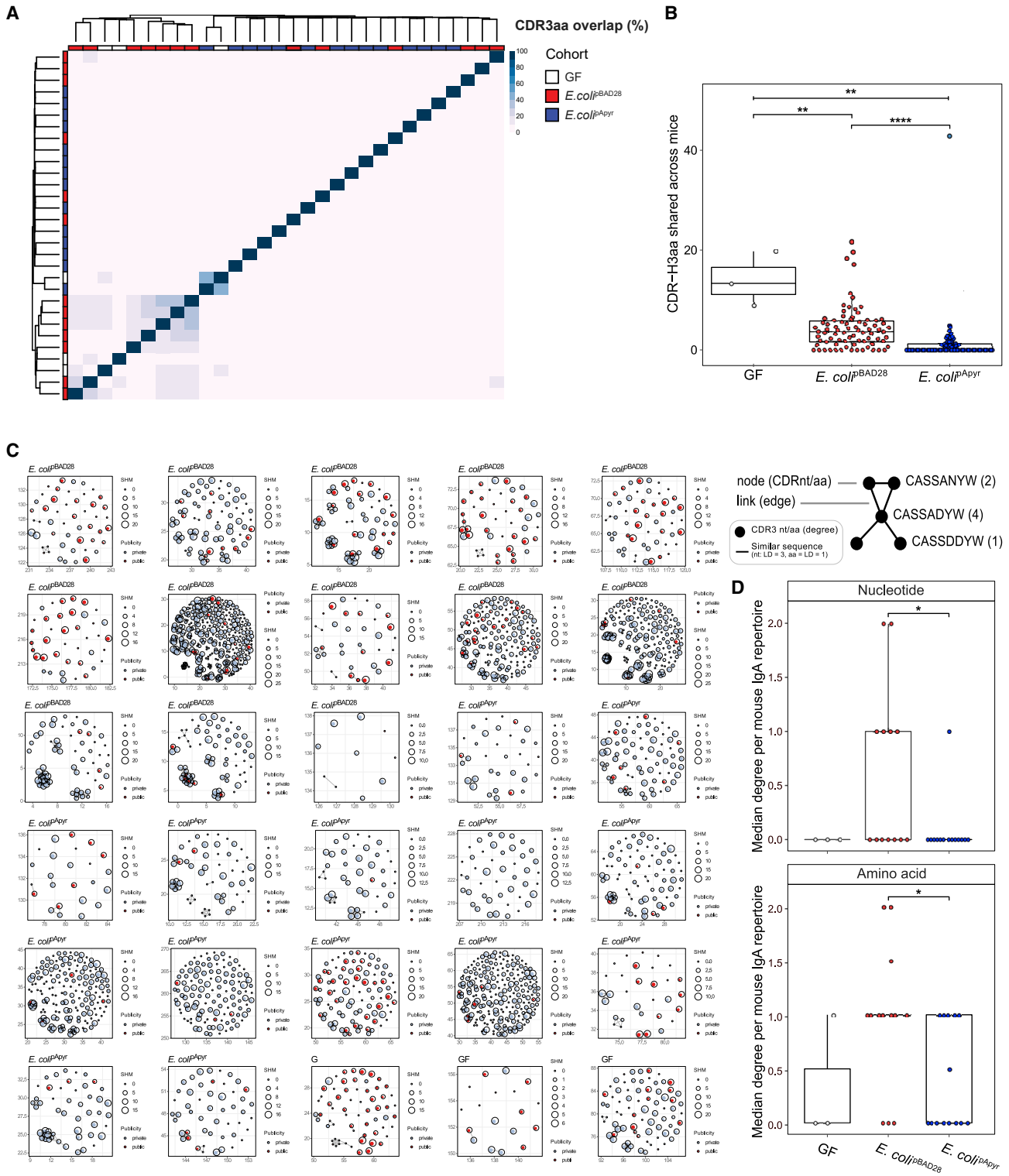

Figure 1. Mice colonized with *E. coli*^{pApyr} develop a more diversified IgA repertoire than mice colonized with *E. coli*^{pBAD28}

Germ-free (GF) C57BL/6 mice were colonized with 10^{10} CFUs of *E. coli*^{pBAD28} or *E. coli*^{pApyr}. Twenty-eight days after colonization, Ig repertoire analysis was performed on IgA^{+} plasma cells isolated from small-intestine lamina propria.

(A and B) Hierarchical clustering (A) and significance analysis (B) of pairwise clonal (CDR3aa) overlap are shown.

(legend continued on next page)

co-evolution selects and maintains mutualistic microorganisms within the gastrointestinal (GI) habitats. Adenosine triphosphate (ATP) is a ubiquitous extracellular messenger, which activates plasma membrane receptors for extracellular nucleotides termed P2 receptors (Burnstock, 2006). Peyer's patches (PPs) are the secondary lymphoid organs within the ileal mucosa, where T cell-dependent IgA responses originate. Most lymphocytes localized in PPs inhabit germinal centers (GCs), where T follicular helper (Tfh) cells interact with B cells and facilitate B cell proliferation, Ig class-switch recombination (CSR), somatic hypermutation (SHM), and affinity maturation (Crotty, 2011). Because Tfh cells in PPs are essential for GC reactions and IgA affinity maturation, they play a critical role in the modulation of the structure and function of intestinal microbial communities (Kawamoto et al., 2014). Tfh cells express high levels of the ionotropic P2X7 receptor (P2X7R) in the plasma membrane; in the PPs, they are exposed to micromolar concentrations of extracellular ATP (eATP) released by the microbiota that permeates the intestinal epithelium. Bacterial eATP limits Tfh cell abundance in PPs via stimulation of P2X7R, thus promoting the generation of a beneficial microbiota via modulation of SIgA response (Proietti et al., 2014). We previously demonstrated that *Escherichia coli* transformants expressing the *phon2* gene from *Shigella flexneri* (*E. coli*^{pApyr}) encoding for the highly active ATP-diphosphohydrolase apyrase efficiently hydrolyses intestinal ATP in both monocolonized and specific pathogen-free (SPF) mice (Perruzza et al., 2017; Proietti et al., 2019); hydrolysis of eATP results in Tfh cell expansion and enhanced B cell help (Perruzza et al., 2017). Here, we investigated whether abrogation of signaling by bacterial eATP affected SIgA repertoire structure and intestinal homeostasis.

RESULTS

Regulation of the SIgA response and repertoire diversity by eATP in the small intestine

In C57BL/6 germ-free (GF) mice colonized with *E. coli*^{pApyr}, hydrolysis of intestinal eATP resulted in enhanced coating of fecal bacteria by SIgA as compared with mice colonized with transformants bearing the empty pBAD28 vector (*E. coli*^{pBAD28}) (Figure S1A); colonization with *E. coli*^{pApyr} resulted in the increase of SIgA in the small intestine, cecum, and colon (Figure S1B). Accordingly, we observed a significant increase of IgA-secreting plasma cells (PCs) by ELISPOT in the intestinal lamina propria (LP) of these mice (Figure S1C). To investigate whether reduction of bacteria-derived ATP could have an impact on the SIgA repertoire, we performed high-throughput sequencing of Ig V_H regions in IgA$^+$ PCs isolated from the LP of gnotobiotic mice colonized with *E. coli*^{pApyr} or *E. coli*^{pBAD28}. Hierarchical clustering analysis of the percentage of IgA CDRH3 amino acid (aa) overlap in PCs from the two groups of animals showed significantly higher overlap among mice colonized with *E. coli*^{pBAD28} than *E. coli*^{pApyr}. The control group of non-colonized GF mice showed the highest CDR3aa overlap (Figures 1A and 1B). These data suggest that colonization with *E. coli*^{pApyr} was associated with more diversified SIgA repertoires between different animals. To further define the architecture of the SIgA repertoire, we performed clonal sequence similarity network analysis (Ben-Hamo and Efroni, 2011; Miho et al., 2019). The number of clones isolated from mice colonized with *E. coli*^{pApyr} or *E. coli*^{pBAD28} did not differ significantly between samples (94–132 clones), as well as the extent of SHM (3.16–4.90 aa mutations). However, *E. coli*^{pBAD28} mice showed a higher degree of clonal expansion of public CDR3 sequences (Li et al., 2020) with respect to *E. coli*^{pApyr} mice, as indicated by a higher abundance of clones with similar sequences within one repertoire; conversely, repertoires isolated from *E. coli*^{pApyr} mice showed a more diverse sequence similarity distribution with less clustering, similarly to the repertoire architecture observed in healthy unimmunized mice (Miho et al., 2019). The sequence similarity within each repertoire was quantified by determining the repertoire's median clonal degree (Greiff et al., 2015) (Figures 1C and 1D). Altogether, these data indicate that reduction of bacteria-derived ATP by apyrase is associated with the generation of a more diversified SIgA repertoire in monocolonized mice.

The breadth of the anti-*E. coli* SIgA response conditions the epithelial transcriptional activity and function in monocolonized mice

We investigated if the enhancement of SIgA coating affected the topography of *E. coli* in the proximal colon. We used SPF C57BL/6 mice expressing E-cadherin^{mCFP} treated with broad-spectrum antibiotics (ABXs) before colonization with *E. coli* as a proxy for gnotobiotic mice. Colonization of these animals with GFP-expressing *E. coli*^{pBAD28} or *E. coli*^{pApyr} showed the distribution of *E. coli*$^{pBAD28/pGFP}$ in closer proximity to the intestinal epithelium as compared with *E. coli*$^{pApyr/pGFP}$ (Figure 2A). No differences were observed in the thickness of the inner mucous layer between differently colonized mice. We detected similar mucous thickness independently of apyrase also in *Igh-J*$^{-/-}$ mice, which carry a deletion in the J segment of the Ig heavy-chain locus and therefore are devoid of Igs (Figure S2B). These data suggest that apyrase does not influence mucous thickness in the colon either in the presence or absence of Igs, and that abrogation of SIgA modulation by eATP modifies *E. coli* interaction with the mucous layer and intestinal epithelium.

Next, we addressed whether apyrase-mediated enhancement of anti-*E. coli* SIgA and modified topography of bacteria had an impact on the transcriptional regulation in intestinal epithelial cells (IECs). We performed genome-wide expression profiling of small intestinal epithelium from GF mice colonized with *E. coli*^{pApyr} or *E. coli*^{pBAD28}. Hierarchical clustering segregated differentially expressed genes in three clusters corresponding to GF, *E. coli*^{pApyr}, and *E. coli*^{pBAD28} gnotobiotic mice (Figure 2B;

(C) Clonal sequence networks for each mouse repertoire were constructed, where nodes represent a CDR3 clonal sequence and edges are drawn if clones differ maximally by 1 aa. Nodes are scaled by mean number of mutations and colored by publicity. Graphical explanation of the clonal sequence networks.
(D) Sequence similarity within each repertoire was quantified by determining the repertoire's mean clonal degree. The degree of a node (clone) indicates the number of similar CDR3 sequences (clones) to a specific CDR3 sequence (node). Data shown are representative of one experiment (n = 3–14).
See also Figures S1A–S1C.

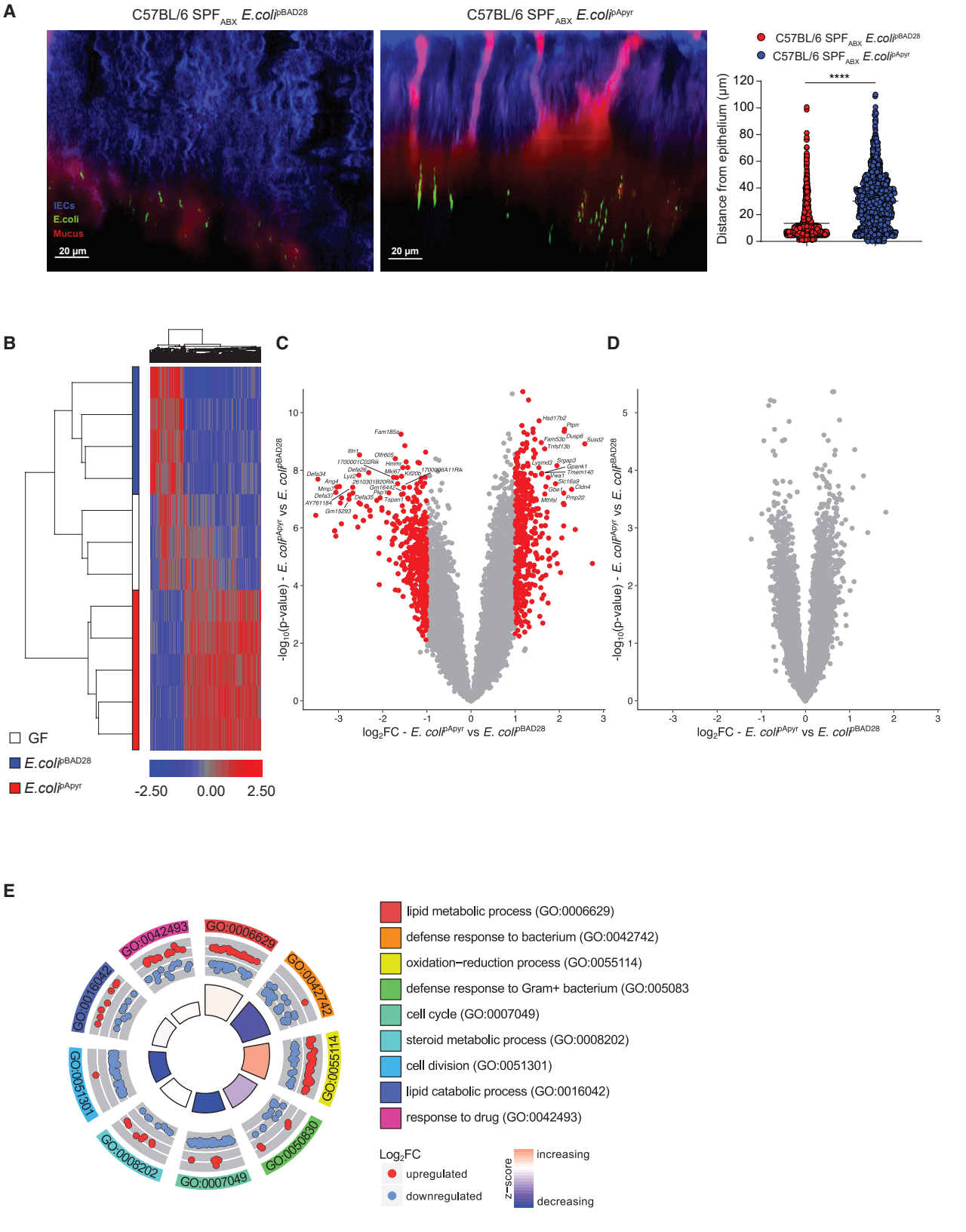

(legend on next page)

Table S1). Whereas a number of genes were differentially expressed in wild-type (WT) mice colonized with *E. coli*^{pApyr} versus *E. coli*^{pBAD28} (false discovery rate [FDR]-corrected $p < 0.05$, $|\log_2FC| > 1$, where $\log_2FC$ represents $\log_2$ fold-change) (Figure 2C; Table S2), strikingly, minimal differences in gene expression were detected between the corresponding *Igh-J*$^{-/-}$ mice (Figure 2D). These data indicate that endoluminal ATP does not substantially affect per se the transcriptional activity of ileal IECs in gnotobiotic mice. In contrast, eATP-mediated shaping of the SIgA response against a commensal bacterium can condition IEC function.

Gene Ontology (GO) enrichment analysis revealed that most of the genes downregulated in IECs from WT mice colonized with *E. coli*^{pApyr} were involved in immunity, including genes related to defense responses against bacteria and cell-cycle regulation (Figures 2E and S2A). In particular, Paneth cell-derived antimicrobial peptide angiogenin 4 (*Ang4*), *Lyz1* and *Lyz2* encoding two isoforms of lysozyme, 14 members of *Defa* family encoding for defensin α isoforms, and their processing enzyme matrix metalloproteinase 7 (*Mmp7*) were all significantly downregulated in IECs conditioned by *E. coli*^{pApyr} with respect to *E. coli*^{pBAD28} (Figure S2A). Moreover, genes involved in the regulation of cell cycle (*Cdk1*, *Cdk4*, and *Cdk20*) and cell division (*Cdc20*, *Bub1b*, and different members of the kinesin family) were downregulated in mice monocolonized with *E. coli*^{pApyr} with respect to *E. coli*^{pBAD28}.

Conversely, key genes involved in metabolic processes governing principally lipid metabolism (*Dgat2*, *Npc1*, *Pparg*, *Cd36*, *Ch25h*, *Apoc2*, and *Apoc3*) and uptake of sugars and glucose (*Slc22a18*, *Slc2a2*, *Slc5a9*, and *Slc5a4*), amino acids (*Slc3a1*, *Slc17a6*, *Slc7a3*, and *Slc1a5*), small peptides (*Slc15a1*), nucleotides (*Slc28a2* and *Slc35a3*), and ions (*Slc12a2*, *Slc6a8*, *Slc40a1*, *Slc30a10*, and *Slc30a2*) were upregulated in WT mice monocolonized with *E. coli*^{pApyr} as compared with *E. coli*^{pBAD28} gnotobiotic mice (Figures 2E and S2A; Table S2). Thus, the downregulation of innate immune genes in IECs by the enhanced SIgA response was counterbalanced by the upregulation of genes involved in metabolic functions. Accordingly, mice monocolonized with *E. coli*^{pApyr} showed increased body weight gain, glycemia, serum insulin, enhanced glucose tolerance, and fat deposition compared with mice colonized with *E. coli*^{pBAD28} (Figures 3A–3F). Consistent with the function of SIgA in controlling these phenomena, no differences in body weight and glucose homeostasis were observed in *Igh-J*$^{-/-}$ mice monocolonized either with *E. coli*^{pBAD28} or *E. coli*^{pApyr} (Figures 3G–3J), suggesting an important role for SIgA in mediating host-microbes immune-metabolic crosstalk.

To understand which cell types were responsible for this differential transcriptional activity, we applied t-statistic stochastic neighbor embedding (t-SNE) overlay of regulated genes on publicly available gene signatures of individual epithelial cells isolated from the small intestine and organoids (Haber et al., 2017) (Figure S2C). The t-SNE overlay revealed the enrichment of the apyrase-induced signature in the mature enterocyte populations (Figure S2D). In particular, the majority of genes that were upregulated in IECs from WT mice colonized with *E. coli*^{pApyr} were expressed in absorptive mature enterocytes (Figures S2E and S2F), while the downregulated genes encoding for anti-microbial peptides and cell-cycle regulators were expressed in particular by Paneth cells and transit-amplifying stem cells, respectively (Figures S2G and S2H). Overall, these data suggest that hydrolysis of eATP by apyrase in the small intestine conditions the symbiotic relationship between the host and microbiota via amplification of the SIgA response.

The breadth of the anti-*E. coli* SIgA response conditions metabolites absorption in the intestine of monocolonized mice

To test if the transcriptional regulation induced in IECs by *E. coli*^{pApyr} had an impact on nutrient absorption, we performed targeted metabolomics analysis of portal vein serum from WT and *Igh-J*$^{-/-}$ gnotobiotic mice. Colonization with *E. coli* irrespective of apyrase expression resulted in a significantly smaller diversity of the metabolic profiles of WT compared with *Igh-J*$^{-/-}$ mice (Figure 4A; Marti Anderson's PERMDISP2 [Permutational Analyses Of Multivariate Dispersions] procedure + permutation test, $p = 0.001$), suggesting SIgA could mediate "metabolic speciation" of the gut ecosystem on microbial colonization. Ig secretion appeared particularly important in regulating lipid

Figure 2. Mouse colonization with *E. coli*^{pApyr} versus *E. coli*^{pBAD28} favors upregulation of genes involved in metabolic functions

(A) Representative images and statistical analysis of bacterial interaction with proximal colon mucosa measured as distance of *E. coli* cells from the epithelial surface in C57BL/6 SPF_{ABX} mice colonized with *E. coli*$^{pApyr/pGFP}$ and *E. coli*$^{pBAD28/pGFP}$. Blue: E-cadherin coupled tog monomeric cyan fluorescent protein (mCFP) in E-cadherin^{mCFP} mice; green: GFP expressing *E. coli*^{pApyr} or *E. coli*^{pBAD28}; red: autofluorescence signal of the mucus obtained by spectral unmixing of the CFP and GFP channels. Two-tailed Mann-Whitney *U* test was used. ****$p < 0.0001$. Representative images are displayed as the maximum intensity projection (MIP) of a full-depth, 10-μm-wide portion of the xz view of the stacks. Data shown are representative of two pooled experiments (n = 7–9).

(B–E) GF C57BL/6 WT and *Igh-J*$^{-/-}$ mice were colonized with 10^{10} CFUs of *E. coli*^{pBAD28} or *E. coli*^{pApyr}. Twenty-eight days after colonization, genome-wide expression profiling was performed on intestinal epithelial cells.

(B) Hierarchical clustering of gene expression profiles in the intestinal epithelium of C57BL/6 GF mice and mice monocolonized with *E. coli*^{pApyr} or *E. coli*^{pBAD28} (FDR-corrected $p < 0.05$ and $\log_2FC > |1.5|$) (see Table S1).

(C) Volcano plot descriptive of differential gene expression in C57BL/6 mice colonized with *E. coli*^{pApyr} versus *E. coli*^{pBAD28}.

(D) Volcano plot descriptive of differential gene expression in *Igh-J*$^{-/-}$ mice colonized with *E. coli*^{pApyr} versus *E. coli*^{pBAD28}. Volcano plots show for each gene (dots) the differential expression ($\log_2$ fold-change [$\log_2FC$]) and its associated statistical significance ($\log_{10}$ p value). The red dots indicate those genes with an FDR-corrected $p < 0.05$ and $\log_2FC > |1|$. We detected 395 upregulated and 411 downregulated genes in mice monocolonized with *E. coli*^{pApyr} as compared with *E. coli*^{pBAD28}. The names of strongly downregulated and upregulated genes (FDR-corrected $p < 10^{-5}$ and $\log_2FC > |1.5|$) are also reported (see Table S2).

(E) Gene Ontology (GO) analysis of the differentially expressed genes (FDR-corrected $p < 0.05$ and $\log_2FC > |1|$) in *E. coli*^{pApyr} versus *E. coli*^{pBAD28} monocolonized C57BL/6 WT mice visualized as GOCircle plot. The inner ring is a bar plot where the height of the bar indicates the significance of the GO term ($\log_{10}$ FDR-corrected p value), and color corresponds to the *Z* score, i.e., the number of genes upregulated minus the number of genes downregulated divided for the square root of the total number of genes analyzed: $z = \frac{(n\ up - n\ down)}{\sqrt{n\ tot}}$. Data shown are representative of a single experiment (n = 4–5).

ABX, antibiotic. See also Figure S2.

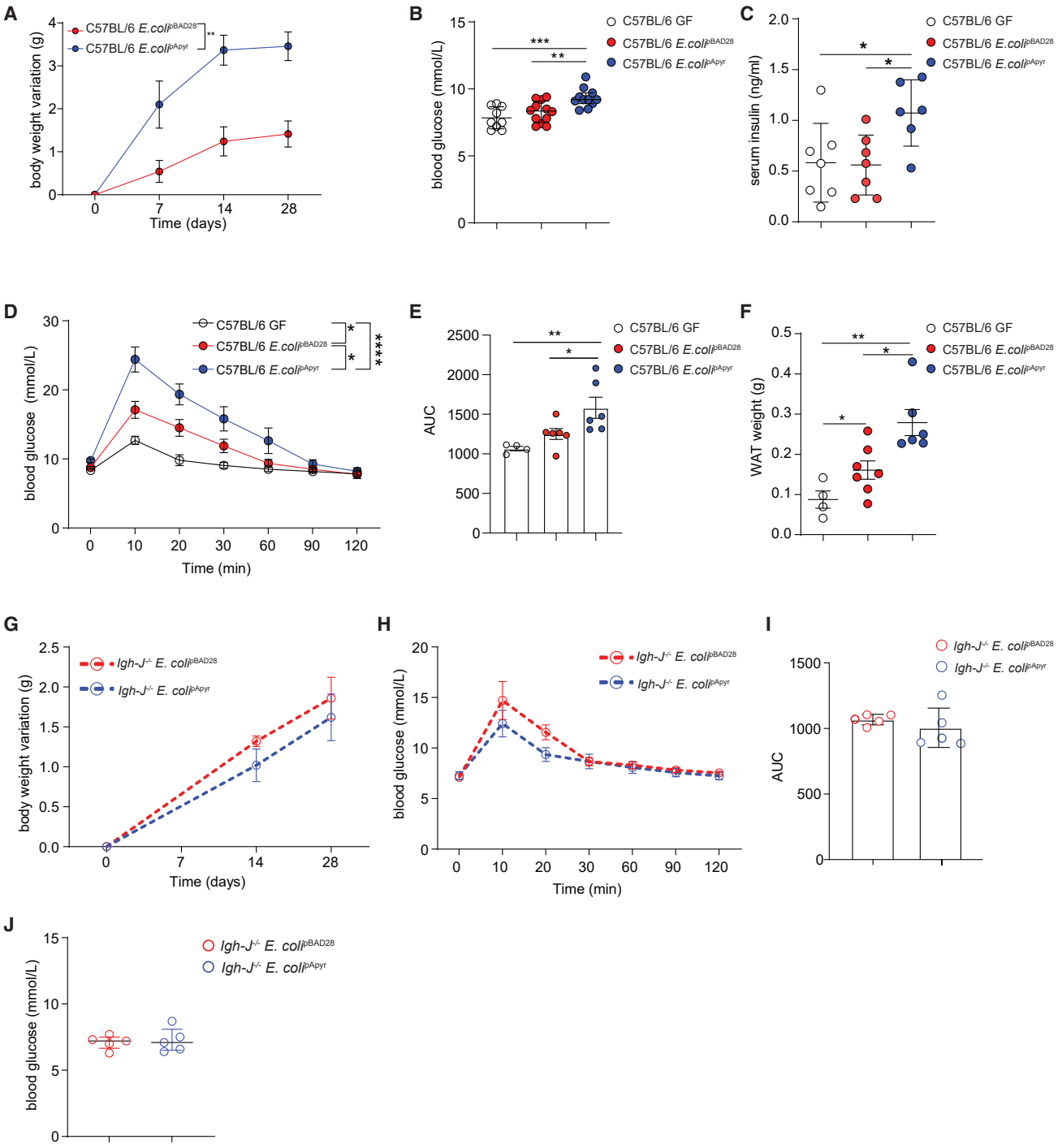

Figure 3. *E. coli*^{pApyr} versus *E. coli*^{pBAD28} monocolonized mice showed improved glucose homeostasis mediated by SIgA

GF C57BL/6 mice were either not colonized or colonized with 10^{10} CFUs of *E. coli*^{pBAD28} or *E. coli*^{pApyr}. Twenty-eight days after colonization, different metabolic parameters were evaluated in the three groups of animals. Data points represent single mice. Except where indicated, one experiment representative of three is shown.

(A) Body weight variation over time (n = 6–7).

(B) Fasting blood glucose analysis from two pooled experiments.

(C) Serum insulin levels.

(D) Glucose tolerance test (GTT) (n = 4–6).

(E) Statistical analysis of the area under the curve (AUC) of (D).

(legend continued on next page)

digestive and absorptive pathways because sphingolipids and glycerophospholipids were enriched in portal vein serum from gnotobiotic WT with respect to *Igh-J*$^{-/-}$ mice (Figure S3A). Next, we focused on the possible role of eATP-mediated shaping of SIgA repertoire structure in conditioning nutrient absorption. *E. coli* colonization had a dominant effect on serum metabolites composition, because colonization with *E. coli*, irrespective of apyrase expression, resulted in rather homogeneous metabolic profiles that were distinct from GF mice (Figure 4B). Nevertheless, the metabolic profiles between the two groups of gnotobiotic animals (i.e., *E. coli*^{pAPyr} and *E. coli*^{pBAD28}) showed few but relevant differences. The univariate analysis performed on the full set of metabolites showed that the significant differences between WT mice colonized with *E. coli*^{pAPyr} and *E. coli*^{pBAD28} were concentrated in specific metabolic classes. Indeed, 8 of 13 aa showed a significantly higher abundance in the portal vein serum of *E. coli*^{pAPyr} mice, as well as three biogenic amines and glycerophospholipids. In contrast, acylcarnitines were enriched in serum collected from *E. coli*^{pBAD28} mice (Figure 4C). These differences were not detected in differently colonized *Igh-J*$^{-/-}$ mice (Figure S3B), suggesting that the alterations in metabolites composition detected in mice conditioned by apyrase were mediated by shaping of the SIgA response against *E. coli*.

Administration of apyrase-expressing bacteria promotes maintenance of gut microbial homeostasis in dysbiosis

SIgA has multiple functions in regulating microbiota composition and gut homeostasis (Weis and Round, 2021). To investigate whether SIgA enhancement by apyrase could beneficially affect gut microbial homeostasis during an environmental perturbation, we used a mouse model of ABX-mediated dysbiosis. A mix of ABXs (vancomycin 1.25 mg, ampicillin 2.5 mg, and metronidazole 1.25 mg) was administered via orogastric gavage to WT mice for 4 consecutive days. After the ABX treatment, mice were orally gavaged for 4 days with PBS (control) or 10^{10} colony-forming units (CFUs) of *E. coli*^{pAPyr} or *E. coli* expressing a loss-of-function isoform of the apyrase enzyme with R192P amino acid substitution (*E. coli*^{pHND19}) (Scribano et al., 2014) (Figure 5A). Quantification of eATP in *E. coli*^{pHND19} and *E. coli*^{pBAD28} cultures showed no significant differences, suggesting that both strains released similar amounts of ATP (Figure S1D). The analysis of metabolic and immunological parameters in ABX-treated mice colonized with *E. coli*^{pHND19} and *E. coli*^{pBAD28} revealed superimposable values, suggesting that both strains produced equivalent effects on gut homeostasis following ABXs administration (Figures S1E–S1O).

Mice treated with ABX alone or in combination with *E. coli*^{pHND19} showed a strong reduction of bacterial taxonomic richness in the cecum as reflected by α-diversity (Shannon index, observed features, and Faith's phylogenetic diversity) (Figure 5B), indicating strong dysbiosis. Interestingly, treatment with *E. coli*^{pAPyr} resulted in a significant improvement of this parameter. To determine similarity in bacterial composition in the different experimental groups, we analyzed β-diversity by principal-coordinate analysis (PCoA) derived from unweighted and weighted UniFrac. Despite each ABX treatment group clustered separately from the untreated control (PERMANOVA <0.001), *E. coli*^{pAPyr}-treated mice clustered closer to the control group, indicating an improved recovery of the physiological microbiota composition (Figure 5C). Relative abundance analysis of differentially represented amplicon sequence variants (ASVs) revealed that that *E. coli*^{pAPyr} administration resulted in the selective preservation of 41 species belonging to the orders of Bacteroidales, Clostridiales, Lactobacillales, and Burkholderiales (Figure 5D). Among Bacteroidales, *Muribaculum intestinale* was detected by multiple ASVs. The reduction of this bacterial species was shown to correlate with higher susceptibility to ileitis (Dobranowski et al., 2019). *E. coli*^{pAPyr} administration favored the preservation of *Clostridium scindens*, a bacterium that was shown to protect from *Clostridioides difficile* infection through the generation of secondary bile acids deoxycholic acid (DCA) and lithocholic acid (LCA). Reconstitution with *C. scindens* alone or within a bacterial consortium protected ABX-treated mice from *C. difficile* intestinal colonization (Buffie et al., 2015). Different species belonging to Lactobacillales order, in particular *Lactobacillus johnsonii* and *Lactobacillus reuteri*, were also significantly enriched in *E. coli*^{pAPyr}-treated mice. These results suggest that apyrase enzymatic function can positively influence gut microbial homeostasis in ABX-mediated dysbiosis. Consistent with SIgA function in mediating the effect of apyrase, the improved recovery in microbiota composition was associated to increased coating of fecal microbiota by SIgA in mice gavaged with *E. coli*^{pAPyr} (Figure 5E).

Administration of apyrase-expressing bacteria attenuates intestinal barrier impairment and glucose homeostasis perturbation in ABX-mediated dysbiosis

ABXs strongly affect microbial diversity and intestinal barrier function, leading to bacterial translocation of live commensal bacteria to the mesenteric lymph nodes (MLNs) (Knoop et al., 2016). A characteristic feature of reduced bacterial load after ABX treatment is cecum enlargement, which characterizes also GF animals (Devkota et al., 2012; Poteres et al., 2020). Analysis of cecum weight 4 days after recovery from ABX treatment revealed a pronounced increase of this parameter, as expected. However, mice treated with *E. coli*^{pAPyr} showed significantly reduced cecum weight as compared with mice treated with

(F) Perigonadal white adipose tissue (WAT) weight.
(G–J) GF *Igh-J*$^{-/-}$ mice were colonized with 10^{10} CFUs of *E. coli*^{pBAD28} or *E. coli*^{pAPyr}. Twenty-eight days after colonization, different metabolic parameters were evaluated in the two groups of animals. Data points represent single mice. One experiment representative of two is shown.
(G) Body weight variation (n = 5).
(H) Glucose tolerance test (GTT) (n = 5).
(I) Statistical analysis of the AUC of (H). (J) Fasting blood glucose analysis.
Means ± SEM are shown. Two-tailed Mann-Whitney *U* test (B, C, E, F, I, and J) and two-tailed ANOVA test (A, D, G, and H) were used. *p < 0.05; **p < 0.01; ***p < 0.001; ****p ≤ 0.0001.

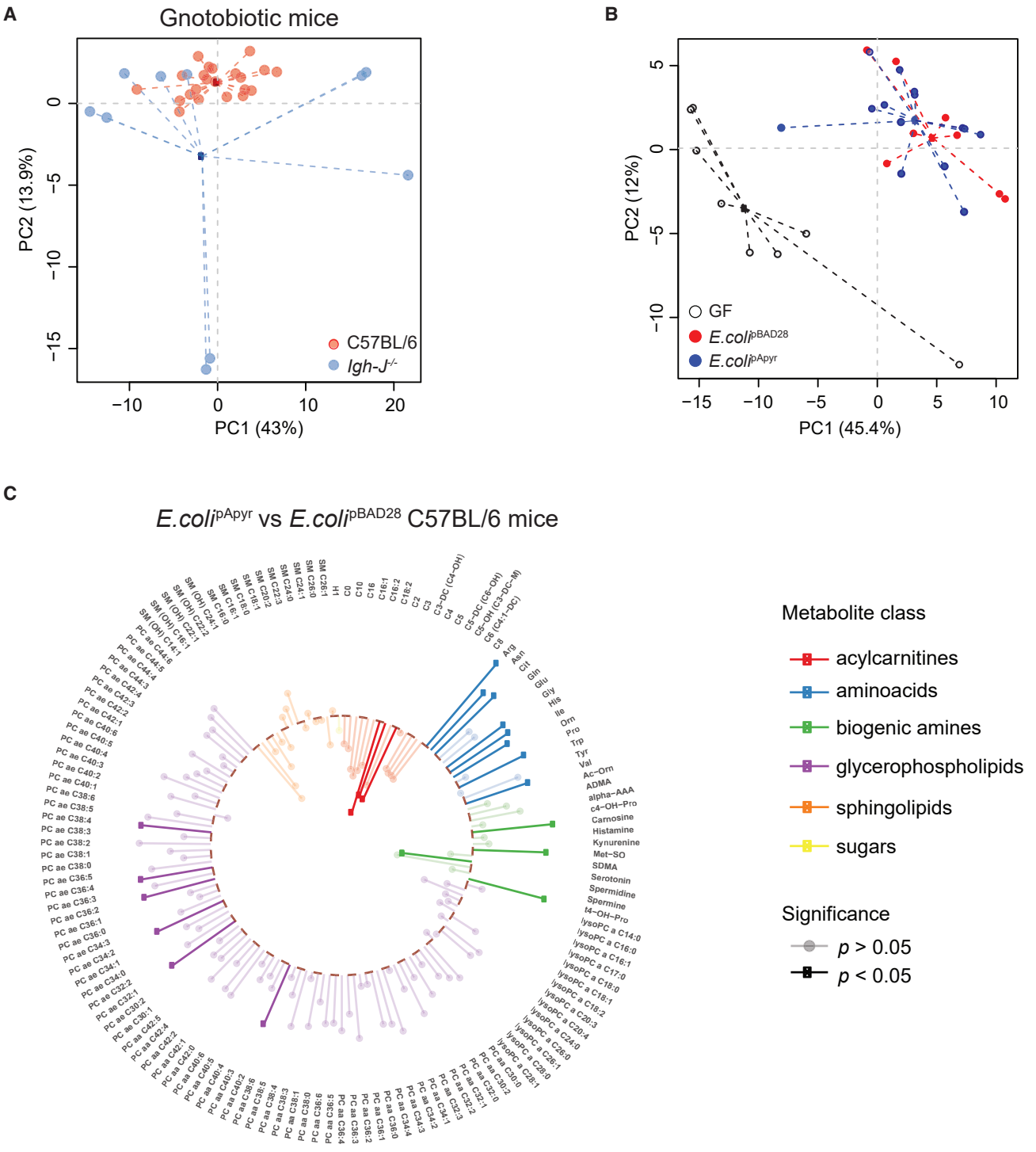

Figure 4. SIgA contributes to bacteria-induced metabolic speciation

Metabolomics analysis performed on portal vein serum of C57BL/6 WT and *Igh-J*$^{-/-}$ mice monocolonized with *E. coli*^{pApyr} or *E. coli*^{pBAD28} transformants. The analysis was performed at 28 days of colonization (n = 7–14). All analyses were performed on log-transformed data. In the PCA score plots, data points indicate the single mice, while centroids highlight the median position of each group.

(A) PCA score plot summarizing the results of the targeted metabolomics analysis of portal vein serum performed on *E. coli* monocolonized C57BL/6 and *Igh-J*$^{-/-}$ mice.

(B) PCA score plot summarizing the results of the targeted metabolomics analysis performed on C57BL/6 WT GF mice and mice monocolonized with *E. coli*^{pApyr} or *E. coli*^{pBAD28}.

(legend continued on next page)

ABX or ABX and *E. coli*^{pHND19} (Figure 5F). Quantification of CFUs from MLN, both in aerobic and anaerobic conditions, revealed a significant increase of bacterial recovery in mice treated with ABX or ABX and *E. coli*^{pHND19} compared with untreated animals, indicating gut barrier integrity was compromised. However, mice treated with the combination of ABX and *E. coli*^{pApyr} showed a number of CFUs in the MLN that was not significantly different from untreated animals (Figures 5G and 5H). These data indicate that *E. coli*^{pApyr} administration mitigates the effects of ABX-induced dysbiosis.

The gut microbiota encodes a more versatile metabolome than the host, and a healthy microbiota is a necessary requirement for stable functional metabolic interactions with the host. To investigate the effect of apyrase on host metabolism perturbation caused by dysbiosis induced by ABXs, we analyzed blood glucose 4 days after recovery from the ABX treatment. Administration of ABXs resulted in a pronounced decrease in blood glucose. Mice treated with apyrase-expressing bacteria showed higher serum glucose levels compared with mice treated with ABX or ABX and *E. coli*^{pHND19} (Figure 5I). Quantification of white adipose tissue (WAT) revealed a significant reduction of WAT in ABX-treated mice both as ABX alone treatment or in association with *E. coli*^{pHND19}. This reduction was significantly attenuated by administration of *E. coli*^{pApyr} (Figure 5J). No improvements in blood glucose levels (Figure S4A) and WAT deposition (Figure S4B) after ABX treatment were observed in *Igh-J*$^{-/-}$ mice treated with *E. coli*^{pApyr} as compared with the counterparts treated with ABX or the combination of ABX and *E. coli*^{pHND19}. These results are consistent with the function of apyrase in attenuating metabolic consequences of ABX-mediated dysbiosis via enhancement of SIgA.

Intestinal conditioning by apyrase promotes resistance to infection by enteric pathogens following ABX treatments

Microbial cells in the GI tract confer colonization resistance against intestinal pathogens. ABX-mediated depletion of endogenous microbes results in increased susceptibility to a number of opportunistic and pathogenic enteric infections (Blaser, 2011; Preidis and Versalovic, 2009). Enterohemorrhagic *E. coli* (EHEC), enteropathogenic *E. coli* (EPEC), and *Citrobacter rodentium* are Enterobacteriaceae that belong to the family of attaching and effacing (A/E) lesion-forming bacteria. EHEC and EPEC can cause severe intestinal inflammation and diarrhea. In addition, EHEC strains expressing the highly potent Shiga toxin (Stx) cause nephrotoxicity, resulting in severe cases in the death of infected individuals. Because the human pathogens EHEC and EPEC induce only modest pathogenicity in ABX-treated adult mice, *C. rodentium* is used to mimic these infections in mice (Collins et al., 2014). We investigated whether apyrase could promote resistance to the challenge of ABX-treated mice with 10^8 CFUs of *C. rodentium* (Figure 6A). Mice gavaged with *E. coli*^{pApyr} after ABXs showed reduced body weight loss on infection as compared with the groups treated with ABX alone or followed by *E. coli*^{pHND19} (Figure 6B). Inflammatory monocytes ($CD45^+CD11b^+Ly6c^+Ly6g^-$ cells) (Figure 6C) and neutrophils ($CD45^+CD11b^+Ly6c^+Ly6g^+$ cells) in the cecum LP (Figure 6D), *C. rodentium* CFUs in both the spleen (Figure 6E) and liver (Figure 6F), and fecal and serum lipocalin-2 (LCN-2) levels (Figures 6G and 6H), which are linked to epithelial damage and neutrophil infiltration, were all significantly reduced in mice treated with *E. coli*^{pApyr} as compared with the groups treated with ABX alone or in combination with *E. coli*^{pHND19}. Notably, *Iga*$^{-/-}$ mice did not show any improvement in intestinal inflammation and control of the infection by combining *E. coli*^{pApyr} administration to the ABX treatment (Figures S4C–S4I), indicating that SIgAs are instrumental in promoting colonization resistance by apyrase.

We further tested the beneficial effect of apyrase in the enteric infection by *C. difficile*. *C. difficile* is a major cause of ABX-associated diarrhea dependent on reduced bacterial community diversity and depletion of key taxa within the intestinal microbiota (Seekatz and Young, 2014). To investigate whether the microbiota community structure induced by apyrase-expressing bacteria could counteract intestinal invasion by *C. difficile*, we administered ABX to WT mice for 4 days to induce microbiota depletion. Thereafter, mice were orally gavaged with *E. coli* transformants for 4 days, infected with 10^5 *C. difficile* VPI 10463 spores, and analyzed 72 h postinfection to evaluate intestinal inflammation (Figure 6I). The loss of body weight (Figure 6J) and the clinical score (Figure 6K) following *C. difficile* infection were both significantly ameliorated by *E. coli*^{pApyr} administration. In mice treated with ABX followed by *E. coli*^{pApyr}, colon length, an important pathological parameter in colitis, was similar to non-infected mice, whereas in mice treated with standalone ABX or in combination with *E. coli*^{pHND19}, it was drastically reduced (Figure 6L). Finally, fecal and serum LCN-2 concentrations were significantly reduced in mice treated with ABX and *E. coli*^{pApyr} as compared with mice treated with ABX alone or in combination with *E. coli*^{pHND19} (Figures 6M and 6N). These data further support the notion that treatment with apyrase-expressing bacteria mitigates ABX-induced dysbiosis and promotes resistance to *C. difficile* infection.

DISCUSSION

The diversity of the SIgA repertoire generated by intestinal B cells does not reflect the complexity of the antigenic universe borne by the microbiota. This phenomenon is consistent with the co-evolution of the gut immune system and microorganisms, and contrasts with the diversification of the systemic B cell repertoire that emerges on exposure to microbial antigens (Li et al., 2020). GCs in PPs from different mice expand public B cell receptor (BCR) clonotypes, some of which are dependent on bacterial antigens, while others are not (Chen et al., 2020). A substantial percentage (5%–10%) of GCs from SPF mice contain highly

(C) Lollipop plot showing the results of the univariate comparison on the metabolic profiles of WT mice colonized with *E. coli*^{pBAD28} or *E. coli*^{pApyr}. The length of the segment is proportional to the difference in the expected values of each metabolite in *E. coli*^{pBAD28} and *E. coli*^{pApyr}. The color highlights the different metabolic classes.
See also Figure S3.

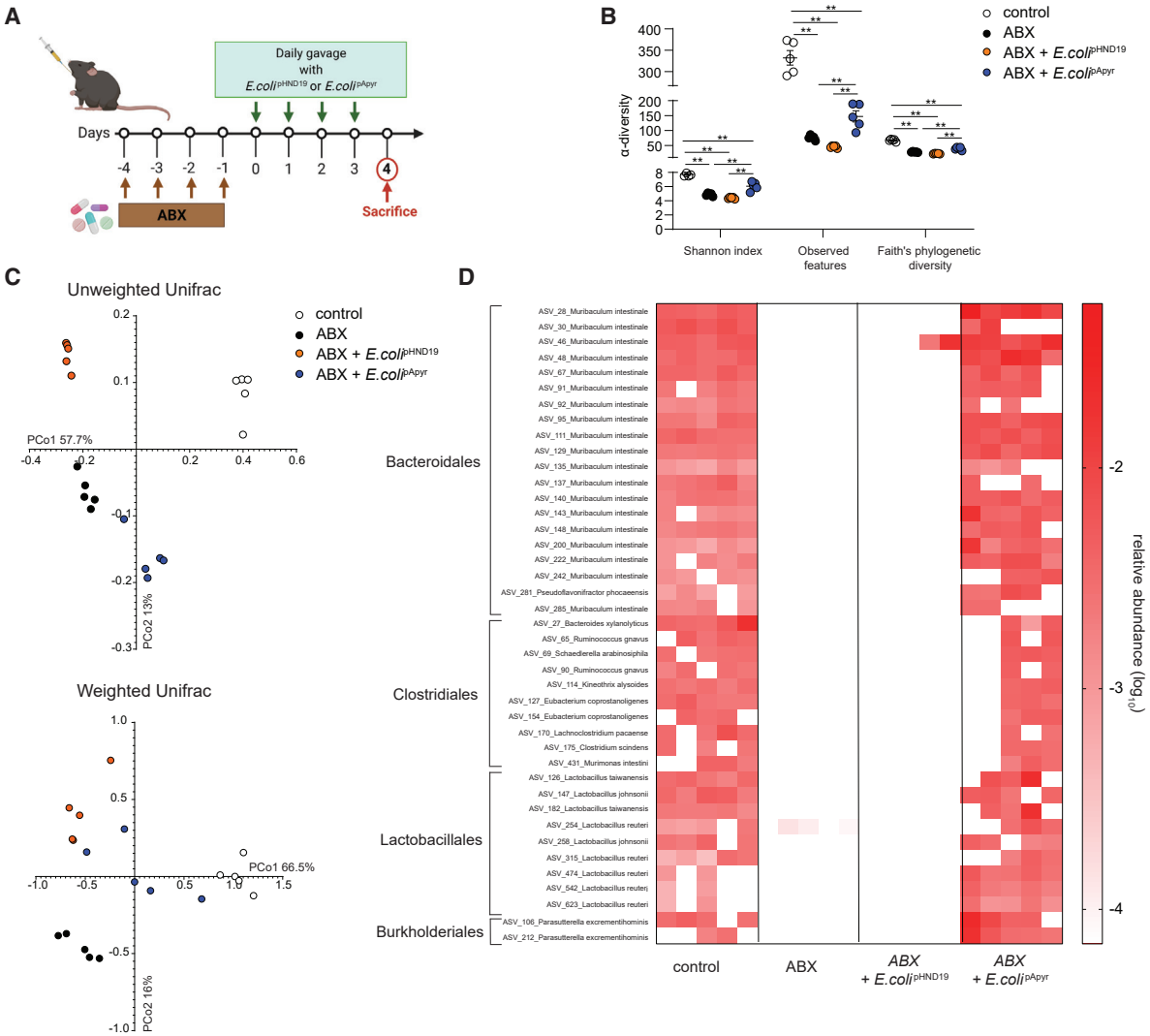

(legend on next page)

dominant B cell clones that are selected by antigens derived from commensal bacteria. The antigen-driven selection of public clonotypes specific for bacterial and non-bacterial antigens appears to be tunable by the presence and composition of the microbiota (Nowosad et al., 2020). The identification of mechanisms responsible for the regulation of the SIgA diversity would allow to intervene for enhancing the efficacy of mucosal vaccination and counteracting disruption of microbiota homeostasis in pathophysiological conditions.

Microbiota-derived eATP limits Tfh cells activity in the PPs via the ATP-gated P2X7R and thereby BCR affinity maturation (Proietti et al., 2014). Hydrolysis of eATP by apyrase delivery to the small intestine resulted in increased SIgA production and higher B cell clonal diversity that was reflected by enhanced coating of intestinal bacteria. SIgA is key in determining a non-inflammatory relationship between the host and microbiota (Peterson et al., 2007). SIgA coating accelerates the small-intestinal transit of bacteria by limiting bacterial motility, by reducing adherence, or by exclusion effects (Uchimura et al., 2018). We found that apyrase-mediated conditioning of SIgA repertoire modified the topographical distribution of bacteria in the mucus, suggesting SIgA shaping by eATP influences bacterial interaction with the epithelium. Accordingly, SIgA generated by an apyrase-bearing live attenuated oral vaccine conferred enhanced protection from the invasiveness of the virulent bacteria (Proietti et al., 2019). Along this line, SIgA generated in mice treated with ABXs and gavaged with *E. coli*^{pApyr} significantly limited both aerobic and anaerobic bacteria translocation to MLN (Figures 5G and 5H).

SIgA plays a central role in conditioning transcriptional activity of the intestinal epithelium. Shulzhenko et al. (2011) have shown that lack of SIgA results in upregulation of immune response genes and concomitant repression of genes correlated with metabolic functions. This shift in intestinal function led to lipid malabsorption and decreased deposition of body fat (Shulzhenko et al., 2011). The enhanced SIgA production by colonization of GF mice with *E. coli*^{pApyr} induced the downregulation of genes involved in immune response against bacteria and upregulation of genes involved in metabolic processes. This effect mediated by apyrase-conditioned SIgA prompted us to characterize metabolites absorption in the portal vein of *E. coli*^{pApyr} monocolonized mice. First, the targeted metabolomic analysis revealed that sphingolipids and glycerophospholipids were particularly enriched in portal vein serum from gnotobiotic WT with respect to antibody-deficient *Igh-J*$^{-/-}$ mice. Second, the upregulation in the intestinal epithelium of genes connected to lipid metabolism and uptake of amino acids that we observed in mice colonized with *E. coli*^{pApyr} with respect to control *E. coli* transformants devoid of apyrase activity correlated with enhanced absorption of glycerophospholipids and essential amino acids. Mucosal conditioning by apyrase induced a significant reduction of serotonin absorption, a biogenic amine indole derivate with pleiotropic function in immune system regulation that was shown to be increased in the small intestine of antibody-deficient mice (Uchimura et al., 2018). Moreover, in *E. coli*^{pApyr} monocolonized mice, we detected an overall reduction of plasma acylcarnitines that are connected with inflammation and insurgence of metabolic disorders (Makrecka-Kuka et al., 2017; Rutkowsky et al., 2014). Therefore, apyrase-mediated enhancement of SIgA diversity and bacterial coating promotes a shift from immune to metabolic functions in the intestinal epithelium.

In SPF mice, modulation of GC reaction in PPs by bacteria-derived eATP via P2X7R in Tfh cells promotes a proficient microbiota for metabolic homeostasis (Perruzza et al., 2017); chronic deregulated SIgA coating of commensal bacteria results in altered systemic metabolism (Perruzza et al., 2019). Conversely, the increase in SIgA diversity in *E. coli*^{pApyr} colonized mice partially compensated the lack of metabolic fitness of GF and monocolonized mice by ameliorating host glucose homeostasis. SIgA coating alters gene expression of mucous-associated bacteria and modulates interphylum interaction (Nakajima et al., 2018). The diversity of antigen targeting by SIgA affects bacterial function and metabolism (Rollenske et al., 2021). Therefore, the apyrase-mediated increase in SIgA diversity could improve the metabolic fitness of *E. coli*^{pApyr}.

SIgA possesses two antithetic functions acting either in preventing or promoting bacterial colonization (Kubinak and Round, 2016). This dichotomy is at least in part driven by characteristic

Figure 5. *E. coli*^{pApyr} administration improves gut microbiome recovery, intestinal barrier integrity, and metabolic homeostasis in ABX-induced dysbiosis

(A–I) Dysbiosis was induced by daily oral gavage of a mix of ABXs for 4 days. After the ABX treatment, during the recovery phase, mice were orally gavaged for 4 days with PBS (control) or 10^{10} CFUs of *E. coli*^{pApyr} or *E. coli*^{pHND19}.

(A) Experimental layout of ABX-induced dysbiosis and recovery phase.

(B) Bacterial α-diversity calculated by Shannon index, observed features, and Faith's phylogenetic diversity. Two-tailed Mann-Whitney *U* test was used. $^{**}p < 0.01$. Data points represent single mice.

(C) Bacterial β-diversity. The PCoA plots of microbial β-diversity were generated using unweighted and weighted UniFrac algorithms. PERMANOVA was used. $p < 0.001$. Data points represent single mice.

(D) Heatmap showing bacterial amplicon sequence variants (ASVs) in cecal microbiota that discriminate the different experimental groups. ASVs were selected according to $p < 0.05$ with Wald test using FDR p value correction following DESeq2 read counts normalization. Each line represents one ASV, and each column represents an individual mouse. Mean relative abundances (log10) of ASVs detected in the different experimental groups are shown.

(E) Statistical analysis of fecal IgA-coated microbiota at the end of the recovery phase (day 4). Microbiota from *Iga*$^{-/-}$ mice was used as negative control for the secondary antibody.

(F) Percentage of cecum weight normalized by total body weight.

(G and H) CFU quantification of aerobic (G) and anaerobic (H) bacteria recovered from the MLN (pooled data from two independent experiments).

(I) Blood glucose variation between day −4 (start of ABX treatment) and day +4 (end of recovery phase).

(J) Percentage of WAT deposition at the end of recovery phase (day 4). Data points represent single mice.

Except where indicated, one experiment representative of three is shown (n = 4–7/experiment). Means ± SEM are shown. Two-tailed Mann-Whitney *U* test (E–I) was used. $^{*}p < 0.05$, $^{**}p < 0.01$. See also Figures S1D–S1O, S4A, and S4B.

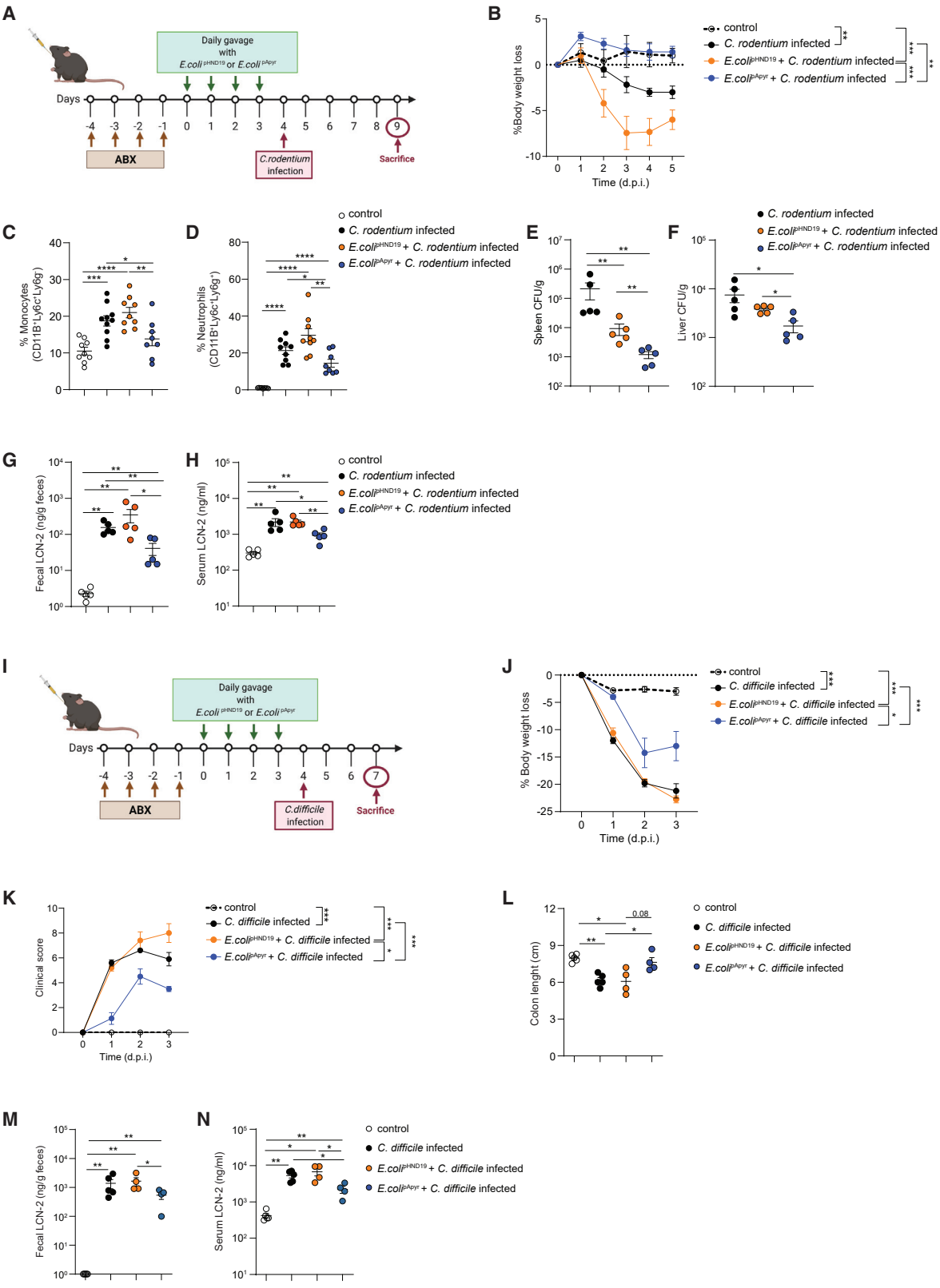

(legend on next page)

features of the bound bacteria, such as the replicative activity, which induces enchained growth and clearance of enteropathogens (Moor et al., 2017). Conversely, SIgA coating of *Bacteroides fragilis* capsular polysaccharides helps bacteria occupy a defined mucosal niche, resulting in exclusion of possibly pathogenic competitors. This phenomenon was shown to be spread across different commensal microbes (Donaldson et al., 2018). ABX treatment results in loss of intestinal microbiota diversity, which requires several weeks to be restored (Palleja et al., 2018), exposing the host to possible colonization by exogenous enteropathogens. Four-day course of an ABX mix renders SPF mice susceptible to enteric infections, including *C. rodentium* and *C. difficile*, two murine models of ABX-mediated human diseases (Becattini et al., 2016). Daily gavage immediately after ABX treatment with *E. coli*^{pApyr}, but not *E. coli*^{pHND19}, expressing a loss-of-function mutant of apyrase, promoted the colonization of different bacterial species belonging to the orders of Bacteroidales, Clostridiales, Lactobacillales, and Burkholderiales that ensured resistance to the infection by *C. rodentium* and *C. difficile.* Among Bacteroidales, *Muribaculum intestinale*, the reduction of which was correlated with higher susceptibility to ileitis (Dobranowski et al., 2019), was detected by multiple ASVs. Notably, *E. coli*^{pApyr} gavaging resulted in the enrichment of *C. scindens* that was previously shown to protect mice from *C. difficile* infection through the generation of the secondary bile acids DCA and LCA (Buffie et al., 2015). Among the Lactobacillales order, *L. johnsonii* and *L. reuteri* were significantly enriched in *E. coli*^{pApyr}-treated mice. These two species are commonly used as probiotics and were shown to confer protection against *C. rodentium* (Mackos et al., 2013) and *Campylobacter jejuni* (Bereswill et al., 2017) infections. Finally, ABX-mediated alteration of glucose metabolism (Zarrinpar et al., 2018) was improved by apyrase-mediated SIgA enhancement. We originally proposed bacteria-derived eATP as an important mediator of gut ecosystem homeostasis by modulating SIgA response (Perruzza et al., 2017; Proietti et al., 2014). The observations reported in the present study suggest that abrogation of eATP signaling and expansion of SIgA diversity by apyrase can be used to restore intestinal microbiota fitness in dysbiotic conditions, such as provoked by ABX treatment.

Limitations of the study

Although our experiments establish a function for apyrase-mediated degradation of luminal ATP in promoting the amplification of the SIgA repertoire in the intestine, the following limitations of the study have to be considered. To analyze the impact of apyrase activity on SIgA structure in a controlled intestinal environment, we used monocolonized mice. In physiological conditions, the complexity of the microbiota and microbiota-derived metabolites might further influence the SIgA repertoire structure and/or bias the response specificity in the absence of eATP. An analogous limitation can be considered for the transcriptional regulation in the epithelial component of the intestine and metabolites absorption by SIgA amplification. The picture we provide, albeit quite explanatory for the role of eATP in regulating intestinal function by shaping the commensal-specific SIgA response, is limited by monocolonization that cannot provide a comprehensive definition of the transcriptional landscape and metabolites absorption of a normally colonized organism. We demonstrated that enhancing the SIgA coating of the microbiota could eventually lead to the attenuation of pathological consequences of dysbiosis induced by ABX treatment. The maintenance of gut homeostasis correlated with the SIgA-dependent preservation of a beneficial bacterial community in mice exposed to apyrase. These experiments were performed in mice housed in an SPF environment; additional studies are warranted to establish the effectiveness of SIgA amplification by apyrase in correcting dysbiosis in non-SPF conditions and in other organisms.

STAR★METHODS

Detailed methods are provided in the online version of this paper and include the following:

- KEY RESOURCES TABLE
- RESOURCE AVAILABILITY
  - Lead contact
  - Materials availability
  - Data and code availability

Figure 6. *E. coli*^{pApyr} administration improves resistance to enteric pathogen infection in ABX-induced dysbiosis

(A–H) Dysbiosis was induced by daily oral gavage of ABXs for 4 days. After the ABX treatment, mice were orally gavaged for 4 days with PBS (control) or 10^{10} CFUs of *E. coli*^{pApyr} or *E. coli*^{pHND19}. Thereafter, mice were orally infected with 10^8 CFUs/mouse of *C. rodentium.*

(A) Experimental layout showing *C. rodentium* infection on ABX-induced dysbiosis.

(B) Percentage body weight loss during 5 days postinfection (dpi) (n = 6–10).

(C) Statistical analysis of inflammatory monocytes ($CD45^+CD11b^+Ly6c^+Ly6g^-$) infiltrating the cecum lamina propria at 5 dpi.

(D) Statistical analysis of neutrophils ($CD45^+CD11b^+Ly6c^+Ly6g^+$) infiltrating the cecum lamina propria at 5 dpi.

(E and F) Quantification of *C. rodentium* dissemination in the spleen (E) and liver (F) at 5 dpi.

(G and H) Quantification of fecal (G) and serum (H) LCN-2 at 5 dpi.

(I–N) Dysbiosis was induced by daily oral gavage of ABXs for 4 days. After the ABX treatment, mice were orally gavaged for 4 days with PBS (control) or 10^{10} CFUs of *E. coli*^{pApyr} or *E. coli*^{pHND19}. Thereafter, mice were orally infected with 10^5 CFUs/mouse of *Clostridioides difficile.* All the different parameters shown are evaluated over 3 dpi.

(I) Experimental layout of *C. difficile* infection on ABX-induced dysbiosis.

(J) Percentage body weight loss (n = 4–5).

(K) Clinical score (n = 4–5).

(L) Colon length (cm) at 3 dpi.

(M and N) Quantification of fecal (M) and serum (N) LCN-2 at 3 dpi.

Data points represent single mice. One experiment representative of three is shown. Means ± SEM are shown. Two-tailed Mann-Whitney *U* test was used (C–H and L–N). Two-way ANOVA was used (B, J, and K). *$p < 0.05$, **$p < 0.01$, ***$p < 0.001$. See also Figures S4C–S4I.

SUPPLEMENTAL INFORMATION

Supplemental information can be found online at https://doi.org/10.1016/j.celrep.2022.111112.

ACKNOWLEDGMENTS

We thank Sara Maffei and the staff of the animal facility of the Institute for Research in Biomedicine and the staff of the clean mouse facility of the University of Bern for excellent mouse husbandry, David Jarossay (Institute for Research in Biomedicine) for cell sorting, and Prof. Siegfried Hapfelmeier (University of Bern) for providing the tetracycline-resistant strain of *C. rodentium* used in this study. This work was supported by the Swiss National Science Foundation (SNSF 310030_192531), the Swiss Cancer League (KFS-5033-02-2020), the Fondazione Ticinese per la Ricerca sul Cancro, the Fondazione San Salvatore, and the Novartis Foundation for Medical-Biological Research (to F.G.).

AUTHOR CONTRIBUTIONS

F.G. conceived and designed the study. F.G. and L.P. designed experiments. F.G., P.F., A.J.M., S.G., and V.G. supervised experiments. L.P., F. Strati, M.R., T.R.-J., and M.P. performed experiments. H.L. performed IgA sequencing. F. Strati and I.K. performed the analysis of gene expression data. G.G. and S.G. performed bacterial taxonomic profiling and analysis. L.P. and D.M. performed two-photon imaging. F. Seehusen performed mucous thickness measurement. F. Strati performed metabolomics sampling. F. Strati, P.S., C.D., and P.F. analyzed metabolomics data. V.G. performed IgA repertoire analysis. F.G., L.P., and F. Strati wrote the manuscript. P.F., A.J.M., S.G., and V.G. revised the manuscript.

DECLARATION OF INTERESTS

F.G. is the founder of MV BioTherapeutics. F.G. and L.P. are inventors in a patent application covering the dysbiosis-correcting effect of apyrase.

Received: January 11, 2022
Revised: May 15, 2022
Accepted: June 28, 2022
Published: July 19, 2022

REFERENCES

Backhed, F., Ley, R.E., Sonnenburg, J.L., Peterson, D.A., and Gordon, J.I. (2005). Host-bacterial mutualism in the human intestine. Science *307*, 1915–1920.

Becattini, S., Taur, Y., and Pamer, E.G. (2016). Antibiotic-induced changes in the intestinal microbiota and disease. Trends Mol. Med. *22*, 458–478.

Ben-Hamo, R., and Efroni, S. (2011). The whole-organism heavy chain B cell repertoire from Zebrafish self-organizes into distinct network features. BMC Syst. Biol. *5*, 27.

Bereswill, S., Ekmekciu, I., Escher, U., Fiebiger, U., Stingl, K., and Heimesaat, M.M. (2017). Lactobacillus johnsonii ameliorates intestinal, extra-intestinal and systemic pro-inflammatory immune responses following murine Campylobacter jejuni infection. Sci. Rep. *7*, 2138.

Blaser, M.J. (2006). Who are we? Indigenous microbes and the ecology of human diseases. EMBO Rep. *7*, 956–960.

Blaser, M. (2011). Antibiotic overuse: stop the killing of beneficial bacteria. Nature *476*, 393–394.

Bolyen, E., Rideout, J.R., Dillon, M.R., Bokulich, N.A., Abnet, C.C., Al-Ghalith, G.A., Alexander, H., Alm, E.J., Arumugam, M., Asnicar, F., et al. (2019). Reproducible, interactive, scalable and extensible microbiome data science using QIIME 2. Nat. Biotechnol. *37*, 852–857.

Buffie, C.G., Bucci, V., Stein, R.R., McKenney, P.T., Ling, L., Gobourne, A., No, D., Liu, H., Kinnebrew, M., Viale, A., et al. (2015). Precision microbiome reconstitution restores bile acid mediated resistance to Clostridium difficile. Nature *517*, 205–208.

Burnstock, G. (2006). Purinergic signalling. Br. J. Pharmacol. *147*, S172–S181.

Buschor, S., Cuenca, M., Uster, S.S., Scharen, O.P., Balmer, M.L., Terrazos, M.A., Schurch, C.M., and Hapfelmeier, S. (2017). Innate immunity restricts Citrobacter rodentium A/E pathogenesis initiation to an early window of opportunity. PLoS Pathog. *13*, e1006476.

Callahan, B.J., McMurdie, P.J., Rosen, M.J., Han, A.W., Johnson, A.J., and Holmes, S.P. (2016). DADA2: high-resolution sample inference from Illumina amplicon data. Nat. Methods *13*, 581–583.

Cerf-Bensussan, N., and Gaboriau-Routhiau, V. (2010). The immune system and the gut microbiota: friends or foes? Nat. Rev. Immunol. *10*, 735–744.

Chen, H., Zhang, Y., Ye, A.Y., Du, Z., Xu, M., Lee, C.S., Hwang, J.K., Kyritsis, N., Ba, Z., Neuberg, D., et al. (2020). BCR selection and affinity maturation in Peyer's patch germinal centres. Nature *582*, 421–425.

Chow, J., Tang, H., and Mazmanian, S.K. (2011). Pathobionts of the gastrointestinal microbiota and inflammatory disease. Curr. Opin. Immunol. *23*, 473–480.

Collins, J.W., Keeney, K.M., Crepin, V.F., Rathinam, V.A., Fitzgerald, K.A., Finlay, B.B., and Frankel, G. (2014). Citrobacter rodentium: infection, inflammation and the microbiota. Nat. Rev. Microbiol. *12*, 612–623.

Crotty, S. (2011). Follicular helper CD4 T cells (TFH). Annu. Rev. Immunol. *29*, 621–663.

Csardi, G., and Nepusz, T. (2006). The Igraph Software Package for Complex Network Research (InterJournal Complex Systems), p. 1695.

Devkota, S., Wang, Y., Musch, M.W., Leone, V., Fehlner-Peach, H., Nadimpalli, A., Antonopoulos, D.A., Jabri, B., and Chang, E.B. (2012). Dietary-fat-induced taurocholic acid promotes pathobiont expansion and colitis in Il10-/- mice. Nature *487*, 104–108.

Dicksved, J., Halfvarson, J., Rosenquist, M., Jarnerot, G., Tysk, C., Apajalahti, J., Engstrand, L., and Jansson, J.K. (2008). Molecular analysis of the gut microbiota of identical twins with Crohn's disease. ISME J. *2*, 716–727.

Dobranowski, P.A., Tang, C., Sauve, J.P., Menzies, S.C., and Sly, L.M. (2019). Compositional changes to the ileal microbiome precede the onset of spontaneous ileitis in SHIP deficient mice. Gut Microb. *10*, 578–598.

Donaldson, G.P., Ladinsky, M.S., Yu, K.B., Sanders, J.G., Yoo, B.B., Chou, W.C., Conner, M.E., Earl, A.M., Knight, R., Bjorkman, P.J., et al. (2018). Gut microbiota utilize immunoglobulin A for mucosal colonization. Science *360*, 795–800.

Fadlallah, J., El Kafsi, H., Sterlin, D., Juste, C., Parizot, C., Dorgham, K., Autaa, G., Gouas, D., Almeida, M., Lepage, P., et al. (2018). Microbial ecology perturbation in human IgA deficiency. Sci. Transl. Med. *10*.

Greiff, V., Bhat, P., Cook, S.C., Menzel, U., Kang, W., and Reddy, S.T. (2015). A bioinformatic framework for immune repertoire diversity profiling enables detection of immunological status. Genome Med. *7*, 49.

Greiff, V., Menzel, U., Haessler, U., Cook, S.C., Friedensohn, S., Khan, T.A., Pogson, M., Hellmann, I., and Reddy, S.T. (2014). Quantitative assessment of the robustness of next-generation sequencing of antibody variable gene repertoires from immunized mice. BMC Immunol. *15*, 40.

Greiff, V., Menzel, U., Miho, E., Weber, C., Riedel, R., Cook, S., Valai, A., Lopes, T., Radbruch, A., Winkler, T.H., et al. (2017). Systems analysis reveals high genetic and antigen-driven predetermination of antibody repertoires throughout B cell development. Cell Rep. *19*, 1467–1478.

Gu, H., Zou, Y.R., and Rajewsky, K. (1993). Independent control of immunoglobulin switch recombination at individual switch regions evidenced through Cre-loxP-mediated gene targeting. Cell *73*, 1155–1164.

Haber, A.L., Biton, M., Rogel, N., Herbst, R.H., Shekhar, K., Smillie, C., Burgin, G., Delorey, T.M., Howitt, M.R., Katz, Y., et al. (2017). A single-cell survey of the small intestinal epithelium. Nature *551*, 333–339.

Harriman, G.R., Bogue, M., Rogers, P., Finegold, M., Pacheco, S., Bradley, A., Zhang, Y., and Mbawuike, I.N. (1999). Targeted deletion of the IgA constant region in mice leads to IgA deficiency with alterations in expression of other Ig isotypes. J. Immunol. *162*, 2521.

Holmes, E., Loo, R.L., Stamler, J., Bictash, M., Yap, I.K., Chan, Q., Ebbels, T., De Iorio, M., Brown, I.J., Veselkov, K.A., et al. (2008). Human metabolic phenotype diversity and its association with diet and blood pressure. Nature *453*, 396–400.

Huang da, W., Sherman, B.T., and Lempicki, R.A. (2009). Systematic and integrative analysis of large gene lists using DAVID bioinformatics resources. Nat. Protoc. *4*, 44–57.

Johansson, M.E., Phillipson, M., Petersson, J., Velcich, A., Holm, L., and Hansson, G.C. (2008). The inner of the two Muc2 mucin-dependent mucus layers in colon is devoid of bacteria. Proc. Natl. Acad. Sci. U SA *105*, 15064–15069.

Kawamoto, S., Maruya, M., Kato, L.M., Suda, W., Atarashi, K., Doi, Y., Tsutsui, Y., Qin, H., Honda, K., Okada, T., et al. (2014). Foxp3(+) T cells regulate immunoglobulin a selection and facilitate diversification of bacterial species responsible for immune homeostasis. Immunity *41*, 152–165.

Knoop, K.A., McDonald, K.G., Kulkarni, D.H., and Newberry, R.D. (2016). Antibiotics promote inflammation through the translocation of native commensal colonic bacteria. Gut *65*, 1100–1109.

Kubinak, J.L., and Round, J.L. (2016). Do antibodies select a healthy microbiota? Nat. Rev. Immunol. *16*, 767–774.

Larsen, N., Vogensen, F.K., van den Berg, F.W., Nielsen, D.S., Andreasen, A.S., Pedersen, B.K., Al-Soud, W.A., Sorensen, S.J., Hansen, L.H., and Jakobsen, M. (2010). Gut microbiota in human adults with type 2 diabetes differs from non-diabetic adults. PLoS One *5*, e9085.

Lee, S.M., Donaldson, G.P., Mikulski, Z., Boyajian, S., Ley, K., and Mazmanian, S.K. (2013). Bacterial colonization factors control specificity and stability of the gut microbiota. Nature *501*, 426–429.

Li, H., Limenitakis, J.P., Fuhrer, T., Geuking, M.B., Lawson, M.A., Wyss, M., Brugiroux, S., Keller, I., Macpherson, J.A., Rupp, S., et al. (2015). The outer mucus layer hosts a distinct intestinal microbial niche. Nat. Commun. *6*, 8292.

Li, H., Limenitakis, J.P., Greiff, V., Yilmaz, B., Scharen, O., Urbaniak, C., Zund, M., Lawson, M.A.E., Young, I.D., Rupp, S., et al. (2020). Mucosal or systemic microbiota exposures shape the B cell repertoire. Nature *584*, 274–278.

Lindner, C., Wahl, B., Fohse, L., Suerbaum, S., Macpherson, A.J., Prinz, I., and Pabst, O. (2012). Age, microbiota, and T cells shape diverse individual IgA repertoires in the intestine. J. Exp. Med. *209*, 365–377.

Lozupone, C., Lladser, M.E., Knights, D., Stombaugh, J., and Knight, R. (2011). UniFrac: an effective distance metric for microbial community comparison. ISME J. *5*, 169–172.

Mackos, A.R., Eubank, T.D., Parry, N.M., and Bailey, M.T. (2013). Probiotic Lactobacillus reuteri attenuates the stressor-enhanced severity of Citrobacter rodentium infection. Infect. Immun. *81*, 3253–3263.

Makrecka-Kuka, M., Sevostjanovs, E., Vilks, K., Volska, K., Antone, U., Kuka, J., Makarova, E., Pugovics, O., Dambrova, M., and Liepinsh, E. (2017). Plasma acylcarnitine concentrations reflect the acylcarnitine profile in cardiac tissues. Sci. Rep. *7*, 17528.

McMurdie, P.J., and Holmes, S. (2013). phyloseq: an R package for reproducible interactive analysis and graphics of microbiome census data. PLoS One *8*, e61217.

Miho, E., Roskar, R., Greiff, V., and Reddy, S.T. (2019). Large-scale network analysis reveals the sequence space architecture of antibody repertoires. Nat. Commun. *10*, 1321.

Moor, K., Diard, M., Sellin, M.E., Felmy, B., Wotzka, S.Y., Toska, A., Bakkeren, E., Arnoldini, M., Bansept, F., Co, A.D., et al. (2017). High-avidity IgA protects the intestine by enchaining growing bacteria. Nature *544*, 498–502.

Nakajima, A., Vogelzang, A., Maruya, M., Miyajima, M., Murata, M., Son, A., Kuwahara, T., Tsuruyama, T., Yamada, S., Matsuura, M., et al. (2018). IgA regulates the composition and metabolic function of gut microbiota by promoting symbiosis between bacteria. J. Exp. Med. *215*, 2019–2034.

Nguyen, L.T., Schmidt, H.A., von Haeseler, A., and Minh, B.Q. (2015). IQ-TREE: a fast and effective stochastic algorithm for estimating maximum-likelihood phylogenies. Mol. Biol. Evol. *32*, 268–274.

Nowosad, C.R., Mesin, L., Castro, T.B.R., Wichmann, C., Donaldson, G.P., Araki, T., Schiepers, A., Lockhart, A.A.K., Bilate, A.M., Mucida, D., et al. (2020). Tunable dynamics of B cell selection in gut germinal centres. Nature *588*, 321–326.

Oksanen, J., Guillaume Blanchet, F., Friendly, M., Kindt, R., Legendre, P., McGlinn, D., Minchin, P.R., O'Hara, R.B., Simpson, G.L., Solymos, P., et al. (2020). Vegan: Community Ecology Package. *R Package Version 2*, pp. 5–7.

Palleja, A., Mikkelsen, K.H., Forslund, S.K., Kashani, A., Allin, K.H., Nielsen, T., Hansen, T.H., Liang, S., Feng, Q., Zhang, C., et al. (2018). Recovery of gut microbiota of healthy adults following antibiotic exposure. Nat. Microbiol. *3*, 1255–1265.

Perruzza, L., Gargari, G., Proietti, M., Fosso, B., D'Erchia, A.M., Faliti, C.E., Rezzonico-Jost, T., Scribano, D., Mauri, L., Colombo, D., et al. (2017). T follicular helper cells promote a beneficial gut ecosystem for host metabolic homeostasis by sensing microbiota-derived extracellular ATP. Cell Rep. *18*, 2566–2575.

Perruzza, L., Strati, F., Gargari, G., D'Erchia, A.M., Fosso, B., Pesole, G., Guglielmetti, S., and Grassi, F. (2019). Enrichment of intestinal Lactobacillus by enhanced secretory IgA coating alters glucose homeostasis in P2rx7(-/-) mice. Sci. Rep. *9*, 9315.

Peterson, D.A., McNulty, N.P., Guruge, J.L., and Gordon, J.I. (2007). IgA response to symbiotic bacteria as a mediator of gut homeostasis. Cell Host Microbe *2*, 328–339.

Poteres, E., Hubert, N., Poludasu, S., Brigando, G., Moore, J., Keeler, K., Isabelli, A., Ibay, I.C.V., Alt, L., Pytynia, M., et al. (2020). Selective regional alteration of the gut microbiota by diet and antibiotics. Front. Physiol. *11*, 797.

Preidis, G.A., and Versalovic, J. (2009). Targeting the human microbiome with antibiotics, probiotics, and prebiotics: gastroenterology enters the metagenomics era. Gastroenterology *136*, 2015–2031.

Proietti, M., Cornacchione, V., Rezzonico Jost, T., Romagnani, A., Faliti, C.E., Perruzza, L., Rigoni, R., Radaelli, E., Caprioli, F., Preziuso, S., et al. (2014). ATP-gated ionotropic P2X7 receptor controls follicular T helper cell numbers in Peyer's patches to promote host-microbiota mutualism. Immunity *41*, 789–801.

Proietti, M., Perruzza, L., Scribano, D., Pellegrini, G., D'Antuono, R., Strati, F., Raffaelli, M., Gonzalez, S.F., Thelen, M., Hardt, W.D., et al. (2019). ATP released by intestinal bacteria limits the generation of protective IgA against enteropathogens. Nat. Commun. *10*, 250.

Rogier, E.W., Frantz, A.L., Bruno, M.E., and Kaetzel, C.S. (2014). Secretory IgA is concentrated in the outer layer of colonic mucus along with gut bacteria. Pathogens *3*, 390–403.

Rollenske, T., Burkhalter, S., Muerner, L., von Gunten, S., Lukasiewicz, J., Wardemann, H., and Macpherson, A.J. (2021). Parallelism of intestinal secretory IgA shapes functional microbial fitness. Nature *598*, 657–661.

Romagnani, A., Vettore, V., Rezzonico-Jost, T., Hampe, S., Rottoli, E., Nadolni, W., Perotti, M., Meier, M.A., Hermanns, C., Geiger, S., et al. (2017). TRPM7 kinase activity is essential for T cell colonization and alloreactivity in the gut. Nat. Commun. *8*, 1917.

Rutkowsky, J.M., Knotts, T.A., Ono-Moore, K.D., McCoin, C.S., Huang, S., Schneider, D., Singh, S., Adams, S.H., and Hwang, D.H. (2014). Acylcarnitines activate proinflammatory signaling pathways. Am. J. Physiol. Endocrinol. Metab. *306*, E1378–E1387.

Scher, J.U., Sczesnak, A., Longman, R.S., Segata, N., Ubeda, C., Bielski, C., Rostron, T., Cerundolo, V., Pamer, E.G., Abramson, S.B., et al. (2013). Expansion of intestinal Prevotella copri correlates with enhanced susceptibility to arthritis. Elife *2*, e01202.

Scribano, D., Petrucca, A., Pompili, M., Ambrosi, C., Bruni, E., Zagaglia, C., Prosseda, G., Nencioni, L., Casalino, M., Polticelli, F., et al. (2014). Polar localization of PhoN2, a periplasmic virulence-associated factor of Shigella flexneri, is required for proper IcsA exposition at the old bacterial pole. PLoS One *9*, e90230.

Seekatz, A.M., and Young, V.B. (2014). Clostridium difficile and the microbiota. J. Clin. Invest. *124*, 4182–4189.

Shulzhenko, N., Morgun, A., Hsiao, W., Battle, M., Yao, M., Gavrilova, O., Orandle, M., Mayer, L., Macpherson, A.J., McCoy, K.D., et al. (2011). Crosstalk between B lymphocytes, microbiota and the intestinal epithelium governs immunity versus metabolism in the gut. Nat. Med. *17*, 1585–1593.

Snippert, H.J., van der Flier, L.G., Sato, T., van Es, J.H., van den Born, M., Kroon-Veenboer, C., Barker, N., Klein, A.M., van Rheenen, J., Simons, B.D., et al. (2010). Intestinal crypt homeostasis results from neutral competition between symmetrically dividing Lgr5 stem cells. Cell *143*, 134–144.

Sommer, F., and Backhed, F. (2013). The gut microbiota–masters of host development and physiology. Nat. Rev. Microbiol. *11*, 227–238.

Team, R.C. (2017). A Language and Environment for Statistical Computing (R Foundation for Statistical Computing).

Turnbaugh, P.J., Hamady, M., Yatsunenko, T., Cantarel, B.L., Duncan, A., Ley, R.E., Sogin, M.L., Jones, W.J., Roe, B.A., Affourtit, J.P., et al. (2009). A core gut microbiome in obese and lean twins. Nature *457*, 480–484.

Uchimura, Y., Fuhrer, T., Li, H., Lawson, M.A., Zimmermann, M., Yilmaz, B., Zindel, J., Ronchi, F., Sorribas, M., Hapfelmeier, S., et al. (2018). Antibodies set boundaries limiting microbial metabolite penetration and the resultant mammalian host response. Immunity *49*, 545–559.e545.

Walter, W., Sanchez-Cabo, F., and Ricote, M. (2015). GOplot: an R package for visually combining expression data with functional analysis. Bioinformatics *31*, 2912–2914.

Weis, A.M., and Round, J.L. (2021). Microbiota-antibody interactions that regulate gut homeostasis. Cell Host Microbe *29*, 334–346.

Wickham, H., Averick, M., Bryan, J., Chang, W., D'Agostino McGowan, N., François, R., Grolemund, G., Hayes, A., Henry, L., Hester, J., et al. (2019). Welcome to the tidyverse. Journal of Open Source Software *4*, 1686.

Wu, H.J., Ivanov, I.I., Darce, J., Hattori, K., Shima, T., Umesaki, Y., Littman, D.R., Benoist, C., and Mathis, D. (2010). Gut-residing segmented filamentous bacteria drive autoimmune arthritis via T helper 17 cells. Immunity *32*, 815–827.

Zarrinpar, A., Chaix, A., Xu, Z.Z., Chang, M.W., Marotz, C.A., Saghatelian, A., Knight, R., and Panda, S. (2018). Antibiotic-induced microbiome depletion alters metabolic homeostasis by affecting gut signaling and colonic metabolism. Nat. Commun. *9*, 2872.

STAR★METHODS

KEY RESOURCES TABLE

REAGENT or RESOURCE	SOURCE	IDENTIFIER
Antibodies		
Anti-mouse B220 Pacific Blue conjugated	BioLegend	Cat.#:103227, clone: RA3-6 B2; RRID:AB_492876
Anti-mouse CD11B PeCy7 conjugated	BioLegend	Cat.#:117318, clone:N418; RRID:AB_493568
Anti-mouse CD19 APCCY7 coniugated	BioLegend	Cat.#:115530, clone: 6D5; RRID:AB_830707
Anti-mouse CD45 FITC conjugated	BioLegend	Cat.#: 103108, clone: 30F11; RRID:AB_312973
Anti-mouse Gr1 PE conjugated	TONBO Bioscience	Cat.#:50-5931, clone: RB6-8C5; RRID:AB_2621803
Anti-mouse Ly6C biotinylated	BioLegend	Cat.#:128004, clone:HK1.4; RRID:AB_1236552
Anti-mouse Ly6G Pacific Blue conjugated	BioLegend	Cat.#:127612, clone: 1A8; RRID:AB_2251161
Rabbit anti-mouse IgA APC conjugated	Brookwood Biomedical, Birmingham, AL, USA	Cat.#: SAB1186; RRID:AB_2921277
Goat anti-mouse IgA alkaline phosphatase (AP) conjugated	Southern Biotech	Cat.#:1040-04; RRID:AB_2794372
Goat anti-mouse IgA biotinylated	Southern Biotech	Cat.#:1040-08; RRID:AB_2794374
Goat anti-mouse IgA FITC conjugated	Southern Biotech	Cat.#:1040-02; RRID:AB_2794370
Goat anti-mouse IgA unlabeled	Southern Biotechnologies	Cat.#:1040-01; RRID:AB_2314669
Goat anti-mouse IgG PECY7 conjugated	BioLegend	Cat.#:405315, clone: Poly4053; RRID:AB_10662421
Goat anti-mouse IgM biotinylated	Southern Biotech	Cat.#:1020-03; RRID:AB_2794199
Mouse IgA unlabeled	Southern Biotech	Cat.#:0106-01; RRID:AB_2714214
Bacterial and virus strains		
Citrobacter rodentium (HA538 strain, Δdadax::tetRA)	(Buschor et al., 2017)	N/A
Clostridioides difficile	ATCC	ATCC® 43255TM
E. coli^{pApyr}	(Scribano et al., 2014)	N/A
E. coli^{pBAD28}	(Scribano et al., 2014)	N/A
*E. coli*p^{HND19}	(Scribano et al., 2014)	N/A
Chemicals, peptides, and recombinant proteins		
Avidin-peroxidase	Sigma-Aldrich	Cat.#:A3151
Streptavidin PerCP	BioLegend	Cat.#:405213
Streptavidin APC	BioLegend	Cat.#:405207
4-Nitrophenyl phosphate disodium salt hexahydrate	Sigma-Aldrich	Cat.#:N2765
Fluorescein isothiocyanate-dextran 4kDa	Sigma-Aldrich	Cat.#:46944
Glucose	Sigma-Aldrich	Cat.#:G7021
Healthpro-X1 glucometer	Axapharm	Cat.#:5788151
L-(+)-Arabinose	Sigma Aldrich	Cat.#:A3256
Luria Bertani broth	Sigma Aldrich	Cat.#:L3022
Ampicillin sodium salt	Sigma Aldrich	Cat.#:A9518
Chloramphenicol	Sigma Aldrich	Cat.#:C0378
American bacteriological agar	Condalab	Cat.#:1802.00
Bovine Serum Albumine	Sigma Aldrich	Cat.#:A7906
BHI Bacto Brain Heart Infusion	Becton Dickinson AG	Cat.#:237500
Taurocholic acid sodium salt hydrate	Sigma Aldrich	Cat.#:T4009
Oxoid^{TM} AnaeroGen^{TM} 2.5L Sachet	Thermo Fisher	Cat.#:AN0025A
Schaedler Agar	Sigma Aldrich	Cat.#:91019

(*Continued on next page*)

Continued

REAGENT or RESOURCE	SOURCE	IDENTIFIER
Vancomycin Hydrochloride, USP Grade	ZellBio GmbH	Cat.#:V-200-5
Metronidazole	Sigma Aldrich	Cat.#:M3761
RPMI Medium 1640(1x)	Gibco	Cat.#:42401-018
Penicillin/streptomycin	Gibco	Cat.#:15070-063
Kanamycin	Gibco	Cat.#:15160-047
EDTA - solution pH 8,0	Axon Lab	Cat.#:A 3145.1000
Collagenase D from *Clostridium histolyticum*	Sigma Aldrich	Cat.#:11088882001
DNAse I grade II	Sigma Aldrich	Cat.#:10104159001
Fetal bovine serum	Gibco	Cat.#:10270-106
Percoll	Cytiva	Cat.#:17089101
Dulbecco's Phosphate Buffered Saline (PBS)	Sigma-Aldrich	Cat.#:D8537
Goat serum	Sigma Aldrich	Cat.#:G9023
SYTO™ BC Green Fluorescent Nucleic Acid Stain	Life Technologies	Cat.#:S34855
3-Amino-9-ethylcarbazole	Sigma Aldrich	Cat.#:A6926
N,N-Dimethylformamide	Sigma-Aldrich	Cat.#:227056
RNAeasy minelute column	Qiagen	Cat.#:74204
RNase-free DNase I	Qiagen	Cat.#:79254
TRIzol Reagent	Thermo Fisher	Cat.#:15596026
SuperScript™ III Reverse Transcriptase	Invitrogen	Cat.#:18080093
RNaseOUT	Invitrogen	Cat. #:10777019
Platinum™ II Taq Hot-Start DNA Polymerase	Invitrogen	Cat.#:14966001
Critical commercial assays		
Biocrates AbsoluteIDQ® p180 Kit	Biocrates life Sciences AG	N/A
Fast DNA Stool Mini Kit	Qiagen	Cat.#:51604
DuoSet ELISA Mouse Lipocalin-2/NGAL	R&D systems	Cat.#:DY1857
High sensitive mouse insulin ELISA kit	Biorbyt Ltd	Cat.#:orb54817
Quant-iT™ PicoGreen™ dsDNA Assay Kits	Thermo Fisher	Cat.#:P7589
RNA miniprep kit	Qiagen	Cat.#:74004
GeneChip® WT Plus Kit	Affymetrix	Cat.#:902281
GeneChip® Hybridization, Wash and Stain Kit	Affimetrix	Cat.#:900299
MiSeq Reagent Kit v2 (500-cycles)	Illumina	Cat.#: MS-102-2003
Deposited data		
16S rRNA amplicon sequences	This paper	ENA: PRJEB49686
IgA sequences	This paper	NCBI BioProject: PRJNA852673
IEC transcriptomic analysis sequences	This paper	NCBI GEO: GSE203433
Experimental models: Organisms/strains		
C57BL/6J	The Jackson Laboratory	JAX stock # 000664
Igh-J$^{-/-}$ (B6.129P2-*Igh-J*^{tm1Cgn}/J)	Jackson Labs (Gu et al., 1993)	JAX stock # 002438
E-cadherin^{mCFP} (B6.129P2(Cg)-*Cdh1*^{tm1Cle}/J)	Jackson Labs (Snippert et al., 2010)	JAX stock # 016933
Iga$^{-/-}$ (*Igha*^{tm1Grh})	SPF Vivarium LASC Schlieren (Harriman et al., 1999)	MGI : 1857185
Oligonucleotides		
V3–V4 hypervariable regions (16S primer) Fwd: 5′- CCT ACG GGN GGC WGC AG -3′	This paper	N/A

(*Continued on next page*)

Continued

REAGENT or RESOURCE	SOURCE	IDENTIFIER
V3–V4 hypervariable regions (16S primer) Rev: 5′- GAC TAC HVG GGT ATC TAA TCC -3′	This paper	N/A
IgA locus 5′-ATCAGGCAGCCGATTATCAC-3′	(Lindner et al., 2012)	N/A
IgA locus 5′-TCTCCTTCTGGGCACTCG-3′	(Lindner et al., 2012)	N/A
IgA locus 5′-TGAATGATGCGCCACTGT-3′	(Lindner et al., 2012)	N/A
constant Cα region 5′-CGTATCGCCTCCCTCGCGCCAT CAG(MID)GAGCTCGTGGGAGTGTCAGTG-3′	(Lindner et al., 2012)	N/A
promiscuous V_H primer 5′-CTATGCGCCTTGCCAGCCC GCTCAGGAGGTGCAGCTGCAGGAGTCTGG-3′	(Lindner et al., 2012)	N/A
Software and algorithms		
FlowJo v10.6.1	BD Bioscience	https://www.flowjo.com/
FACSDiva	BD Bioscience	N/A
GraphPad Prism	Graphpad Software	https://www.graphpad.com
R studio	Rstudio, Inc	Version 4.0.3
R package *"GOplot"*	(Walter et al., 2015)	https://github.com/wencke/wencke.github.io
R package "Phyloseq"	(McMurdie and Holmes, 2013)	https://github.com/joey711/phyloseq
R package "Vegan"	(Oksanen et al., 2020)	https://cran.r-project.org, https://github.com/vegandevs/vegan
R package "Tidyverse and ggplot"	(Wickham et al., 2019)	https://cloud.r-project.org/package=ggplot2
MiXCR software package v.3.04	(Greiff et al., 2017)	N/A
Partek Genomics Suite (v6.6)	Parteck	https://www.partek.com/partek-genomics-suite/
DAVID Bioinformatics Resources (v6.8)	(Huang da et al., 2009)	https://david.ncifcrf.gov)
Fiji	ImageJ	Version 1.51 s
QIIME 2 2020.2	(Bolyen et al., 2019)	https://qiime2.org
DADA2	(Callahan et al., 2016)	https://github.com/benjjneb/dada2
IQ-TREE stochastic algorithm	(Nguyen et al., 2015)	N/A

RESOURCE AVAILABILITY

Lead contact

Further information and requests for resources and reagents should be directed to and will be fulfilled by the Lead Contact, Fabio Grassi (fabio.grassi@irb.usi.ch).

Materials availability

This study did not generate new unique reagents.

Data and code availability

- Gene expression data on intestinal epithelial cells have been deposited in NCBI GEO and are accessible under the number GSE203433. Sequence reads from 16S rRNA gene profiling have been deposited in the European Nucleotide Archive (ENA) of the European Bioinformatics Institute under the accession number of the study ENA: PRJEB49686. IgA sequencing data are available at NCBI in the BioProject database with accession number BioProject: PRJNA852673.
- This paper does not report original code.
- Any additional information required to reanalyze the data reported in this paper is available from the lead contact upon request.

EXPERIMENTAL MODEL AND SUBJECT DETAILS

Mice

Germ free (GF) C57BL/6 and *Igh-J*$^{-/-}$ (B6.129P2-Igh-Jtm1Cgn/J) and mice were maintained in flexible film isolators at the Clean Animal Facility, University of Bern, Switzerland until experiments. Later, 6 weeks old GF animals were colonized with a single administration of 10^{10} CFU of *E. coli*^{pApyr} or *E. coli*^{pBAD28} by oral gavage in 200 μl PBS and maintained in germ-free isolators located at

the Institute for Research in Biomedicine, Bellinzona, Switzerland, for 28 days before experiments. Specific pathogen-free (SPF) C57BL/6, *Igh-J*$^{-/-}$ (B6.129P2-*Igh-J*^{tm1Cgn}/J), *Iga*$^{-/-}$ (*Igha*^{tm1Grh}) and *E-cadherin*^{mCFP} (B6.129P2(Cg)-*Cdh1*^{tm1Cle}/J) animals were bred at the Institute for Research in Biomedicine, Bellinzona, Switzerland. For all the experiments, mice were used at 4-8 weeks old, age-and sex-matched. Animals were housed in ventilated cages in a 12 h light/dark cycle, with free access to water and standard autoclaved chow.

For FITC-dextran intestinal permeability studies, mice were fasted for 4 h and gavaged with FITC-dextran (0.6 mg/g body weight) diluted in PBS. Serum was collected 4 h post-gavage and fluorescence intensity was measured at 485/530 nm using a micro-plate reader (Biotek Synergy 2). Glucose tolerance test was performed as follow: animals were fasted for 12 h and then received an intra-peritoneal injection of glucose (2 g/kg of body weight). Blood glucose was measured using a glucometer (Healthpro-X1, Axapharm) on samples collected from tail vein. For *ex vivo* experiments, mice were euthanized by CO_2 inhalation and three portions of duodenum, jejunum and ileum, Peyer's patches, white perigonadal adipose tissue, faeces, small intestinal and caecal contents were collected.

Insulin in serum was quantified using an ELISA kit (High sensitive mouse insulin ELISA kit, Biorbyt Ltd). All animal experiments were performed in accordance with the Swiss Federal Veterinary Office guidelines and authorized by the Cantonal Veterinary. Animals were cared for by a licensed veterinarian and proper steps were taken to ensure the welfare and minimize the suffering of all animals in the conducted studies.

Bacterial strains and culture conditions

Full-length *phoN2*::HA fusion, encoding periplasmic ATP-diphosphohydrolase (apyrase) of *Shigella flexneri* M90T, was cloned into the polylinker site of pBAD28 plasmid, under the control of the pBAD L-arabinose inducible promoter, generating plasmid pHND10 and pHND19 (Scribano et al., 2014). In contrast to the pHND10 plasmid, the pHND19 plasmid (control) contains a *phoN2*$_{R192P}$::HA fusion, which encodes a loss-of-function isoform of apyrase carrying the R192P substitution. *E. coli* DH10B transformed with pBAD28 (*E. coli*^{pBAD28}), pHND19 (*E. coli*^{PHND19}) or pHND10 (*E. coli*^{pApyr}) were grown in LB broth supplemented with L-arabinose (0.03%), ampicillin (100 μg/ml) and chloramphenicol (30 μg/ml) at 37°C, 220 rpm. The pBAD promoter is constantly active in the mouse gut lumen (Perruzza et al., 2019). The tetracycline-resistant HA538 strain (Δ*dadx::tetRA*) of *Citrobacter rodentium* (Buschor et al., 2017) was cultured in LB agar plates supplemented with tetracycline (12.5 μg/ml) and then expanded in Luria broth overnight at 37°C. *Clostridioides difficile* ATCC® 43255TM (VPI 10463 $A^+B^+CDT^-$) spores were stocked at 10^8/ml at -80 °C in PBS + 1% BSA. Spores titres were confirmed by plating serial dilutions of the stocks on brain heart infusion (BD Biosciences) agar plates supplemented with 5 g/l yeast extract and 0.1% taurocholate to induce germination. Plates were kept at least 24 h in airtight canisters equipped with Oxoid Anaerogen^{TM}. For calculation of colony forming units (CFU) in the MLN after antibiotic induced dysbiosis mice were sacrificed at the end of the experiment, MLN were harvested aseptically into RPMI and mechanically homogenized. Dilutions of homogenates were plated onto Schaedler agar (Sigma Aldrich). Plates were grown under aerobic or anaerobic culture con For determination of total *C. rodentium* loads, homogenates of spleen and liver, collected at 5 days post infection, were plated on LB agar plates containing 12.5 μg/ml of tetracycline and placed at 37°C for 24 h before enumeration of colonies.

METHOD DETAILS

Generation of SPF$_{ABX}$ mice

4 weeks old C57BL/6 or *E-cadherin*^{mCFP} animals were orally gavaged with a mix of antibiotics (ABX: Vancomycin 1,25 mg, ampicillin 2,5 mg and metronidazole 1,25 mg) in 200 μl water for 2 weeks. After the ABX treatment, these animals were daily gavaged with 10^{10} CFU of *E. coli*^{pBAD28} or *E.coli*^{pHND19} (Figures S1E–S1O) or 10^{10} CFU of GFP expressing *E. coli*^{pApyr} or *E. coli*^{pBAD28} (Figure 2A) in 100 μl PBS for 21 days to ensure intestinal colonization.

Mouse model of antibiotic mediated dysbiosis

Dysbiosis was induced in 6-8 weeks old C57BL/6 or *Igh-J*$^{-/-}$ mice by daily oral gavage of a mix of antibiotics (ABX: Vancomycin 1,25 mg, ampicillin 2,5 mg and metronidazole 1,25 mg; in 200 μl sterile water per mouse) for 4 days. After the antibiotic treatment, during the recovery phase, mice were orally gavaged for 4 days with PBS (control) or 10^{10} CFU (colony forming unit) of *E. coli*^{pApyr} *or E. coli* expressing the loss-of-function isoform of apyrase with the R192P amino acid substitution *(E. coli*^{pHND19}). The treatment schedule is shown in Figure 5A.

Citrobacter rodentium infection model

8-week old C57BL/6 mice were randomly assigned to 4 different experimental groups (see Figure 6A for experimental layout): not treated (control), treated with antibiotics (ABX: Vancomycin 1,25 mg, ampicillin 2,5 mg and metronidazole 1,25 mg; in 200 μl sterile water per mouse), treated with ABX and 10^{10} CFU of *E. coli*^{pHND19}; and treated with ABX and 10^{10} CFU of *E. coli*^{pApyr}. After the antibiotic treatment, mice were orally gavaged for 4 days with PBS (control); or 10^{10} CFU of *E. coli*^{pHND19}; or *E. coli*^{pApyr}. Thereafter, mice were orally infected with 10^8 CFU/mouse of *Citrobacter rodentium*. For infection experiments, a tetracycline-resistant strain of *Citrobacter rodentium* (HA538 strain, Δdadax::tetRA) (Buschor et al., 2017) was cultured in LB agar plates supplemented with tetracycline (12.5 μg/ml) and then expanded in Luria broth overnight at 37°C.

Clostridioides difficile infection model

8-week old C57BL/6 mice were randomly assigned to 4 different experimental groups (see Figure 6E for experimental layout): not treated (control), treated with antibiotics (ABX: Vancomycin 1,25 mg, ampicillin 2,5 mg and metronidazole 1,25 mg; in 200 μl sterile water per mouse), treated with ABX and 10^{10} CFU of *E. coli*^{pHND19}; and treated with ABX and 10^{10} CFU of *E. coli*^{pApyr}. After the antibiotic treatment, mice were orally gavaged for 4 days with PBS (control); or 10^{10} CFU of *E. coli*^{pHND19}; or *E. coli*^{pApyr}. Thereafter, mice were orally infected with 10^5 *C .difficile* VPI 10463 spores. To this end, *Clostridioides difficile* ATCC® 43255TM (VPI 10463 $A^+B^+CDT^-$) spores were stocked at 10^8/ml at -80°C in PBS + 1% BSA. Spores titres were confirmed by plating serial dilutions of the stocks on brain heart infusion (BD Biosciences) agar plates supplemented with 5 g/l yeast extract and 0.1% taurocholate to induce germination. Plates were kept at least 24 h in airtight canisters equipped with Oxoid Anaerogen™. The clinical score used in *Clostridioides difficile* infection is shown in Table S3.

Cells purification and flow cytometry

For intestinal lamina propria cells purification, small intestine was washed trice with ice cold PBS and digested at 37°C for 30 min with RPMI added with 5 mM EDTA for two times. The filtrated fragments were then digested in RPMI 5% FBS (fetal bovine serum), 1 mg/ml collagenase D from *Clostridium histolyticum* 100 mg (Roche Diagnostics) and 40 μg/ml DNase-I grade II (Roche Diagnostics) for 40 min. The filtered suspension, containing the lamina propria cells, was centrifuged for 5 min at 1500 rpm and resuspended in 40% Percoll (Sigma-Aldrich). 80% Percoll was delicately added to samples using a Pasteur pipette, which were then centrifuged for 20 min at 2000 rpm, at room temperature without acceleration and brake. The leukocytes ring formed at the interface between 40% and 80% Percoll was collected, resuspended in FBS, homogenized, centrifuged for 5 min at 1500 rpm and finally resuspended in RPMI complete medium. Single-cell suspensions from intestinal lamina propria were stained with labelled antibodies diluted in PBS with 2% FBS for 20 min on ice. For analysis of inflammatory infiltrates in caecum lamina propria after *C. rodentium* infection, caecum was removed, opened longitudinally, delicately separated by caecal content and washed trice with ice cold PBS. The caecum was digested as explained above for the small intestine lamina propria cells. The filtered suspension, containing the caecum lamina propria cells, was centrifuged for 5 min at 1500 rpm and resuspended in RPMI complete medium. Single-cell suspensions from caecal lamina propria were stained with labelled antibodies diluted in PBS with 2% FBS for 20 min on ice. All antibodies used for flow cytometry are listed in the key resources table. For analysis of IgA coated bacteria in flow cytometry, fresh faecal pellets were collected into sterile 2mL tubes and homogenized in PBS (0.1 g/ml). The homogenized samples were centrifuged at 400 g for 5 min to remove large debris. Supernatants were centrifuged at 8'000g for 10 min to remove unbound IgAs. Bacterial pellets were resuspended in PBS 5% goat serum (Jackson Immunoresearch, West Grove, PA, USA), incubated 15 min on ice, centrifuged and resuspended in PBS 1% BSA for staining with APC conjugated rabbit anti-mouse IgA antibodies. After 30 min incubation, bacteria were washed twice and resuspended in 2% paraformaldehyde in PBS for acquisition at LSRFortessa. For analysis, forward and side scatter parameters were used in logarithmic mode. SYBR Green was added to identify bacteria-sized particles containing nucleic acids. *Rag1*$^{-/-}$ mice were used as control for absence of Igs-coated bacteria. Samples were acquired on an LSR Fortessa (BD Biosciences, Franklin Lakes NJ, USA) flow cytometer. Data were analyzed using the FlowJo software (TreeStar, Ashland, OR, USA) or FACS Diva software (BD Biosciences, Franklin Lakes NJ, USA).

ELISPOT assay

Frequency of small intestine lamina propria secreting IgA plasmacells were detected using an ELISPOT assay. Briefly, 96-well plates (Millipore) were coated with 5 μg/ml purified goat anti-mouse IgA (Southern Biotechnologies). After washing and blocking with 1% BSA in PBS for 30 min, serial dilutions of total small intestine lamina propria cells were added and incubated at 37°C for 16 h. The plates were washed and incubated with anti-IgA biotin-conjugated secondary antibodies, followed by streptavidin HRP (Sigma-Aldrich). The assay was developed with AEC (Sigma-Aldrich). Spot counting was performed using C.T.L. S6 Ultra-V Analyzer Immunospot.

ELISA assay

Small intestine, caecum and fecal samples were collected and processed. Briefly, fresh fecal pellets were collected into sterile 1.5 mL Eppendorf tubes and homogenized in PBS (0.1 g/ml). The samples were then centrifuged for 10 min at maximum speed. The centrifugation process was repeated for two consecutive times and supernatant was stored at -20°C till use. Concentration of total amount of IgA in the different biological samples were detected by ELISA. ELISA plates (Corning half-area 96 well plate) were coated (16 h at 4°C) with 25 μL of unlabeled goat anti-murine IgA, (Southern Biotech) at 5 μg/ml in PBS, washed 4 times with PBS 0.025% Tween 20 and saturated with 50 μl of PBS 1% BSA (Sigma) for 1 h at room temperature. Twenty-five μl of serial dilutions of the different samples were incubated 2 h at room temperature. After 4 washes in PBS 0.025% Tween 20, 25 μl of alkaline-phosphatase conjugated goat anti-mouse IgA, (Southern Biotech) (1:500 in PBS 1% BSA) were added and plates were incubated for 2 h at room temperature. The assay was developed with 4-Nitrophenyl Phosphate disodium salt hexahydrate (Sigma) in carbonate buffer and absorbance was detected at 405 nm.

Lipocalin-2 quantification

The inflammation status of mice was evaluated by measuring the levels of Lipocalin-2 (LCN-2) in fecal supernatants via ELISA assay (R&D systems, DuoSet ELISA Mouse Lipocalin-2/NGAL). Briefly, fresh fecal pellets were collected into sterile 1.5 mL Eppendorf tubes

and homogenized in PBS (0.1 g/ml). The samples were then centrifuged twice for 10 min at maximum speed and the supernatant was stored at -20°C till use. Adequate serial dilution of fecal samples were used to perform the LCN-2 ELISA assay following the manufacturer's suggestion. Absorbance was read at 405 nm and the LCN-2 concentration obtained was normalized for the dilution factor and for stools weight.

High-throughput sequencing of Ig V_H regions and data analysis

The repertoire sequencing of LP IgA^+ plasmacells (PCs) (sorted as $B220^-CD19^+IgA^+IgM^-IgG^-$) was performed following a previous literature with minor modifications (Li et al., 2020). In brief, sorted cells frozen in buffer RLT (RNA miniprep kit, Qiagen) were allowed to thoroughly thaw by staying at RT for 30 min. Thawed samples were immediately vortexed for 30 s to homogenize, and one time (v/v) 70% EtOH was added to each of the sample. After passing all RNA containing liquid through RNAeasy minelute column, 70 μl of RNase-free DNase I (Qiagen) was applied to the column to remove leftover gDNA. Column was then washed by sequential buffer RW, buffer RPE and 80 % EtOH, and RNA was eluted by addition of 14 μl RNase/DNase free water. cDNA synthesis was done by mixing 11 μl of RNA sample, 1 μl of 2 μM IgA isotype gene-specific primer mix (Lindner et al., 2012), 1 μl of 10 mM of dATP, dCTP, dGTP and dTTP (Invitrogen). Samples were then heated to 65 °C for 5 min and cooled down for 1 min on ice, and 4 μl 5× first strand buffer (Invitrogen), 1 μl 0.1 M DTT (Invitrogen), 1 μl RNaseOUT (Invitrogen) and 1 μl Superscript III RT enzyme (Invitrogen) were added to the reaction. After blending, reactions were incubated at 55 °C for 50 min. The reaction was inactivated by heat at 85 °C for 5 min. Samples were stored at −20 °C until further processing. Amplicons of IgA immunoglobulin heavy chain were obtained by PCR using forward primer mix and IgA specific reverse primer with PlatinumTaq (Qiagen), in a total volume of 50 μl. The forward primer mix is composed of 19 different primers binding into FR1 as previously described (Greiff et al., 2014). Before sequencing, amplicons were barcoded according to sample resource and pooled for sequencing on the Illumina MiSeq platform (2 × 250 cycles, paired-end) with 10% PhiX control library. Mean base-call quality was monitored by limiting the Phred score < 30. The resulting FASTQ files were preprocessed (VDJ alignment and CDR3 annotation) and error-corrected using the MiXCR software package v.3.04 using C57BL/6J germline gene data (Greiff et al., 2017). For all analyses, clones were defined by 100% amino acid sequence identity of CDR3 regions. Clones were defined as public if their CDRH3aa sequences were shared at least twice within a given mouse cohort (Germ Free, *E. coli*^{pBAD28} and *E. coli*^{pApyr}).

Quantification of clonal overlap

Pairwise clonal overlap between repertoires A and B was calculated as: Shared clones(A,B) % = $A \cap B$ / mean(|A|,|B|) *100. where $A \cap B$ is the absolute number of shared clones and |A| and |B| signify the number of clones (CDRH3aa) in repertoire A and B, respectively.

Network similarity analysis

Networks of CDR3aa sequences were constructed as previously described (Miho et al., 2019). Briefly, for each repertoire, a network was drawn using the R package igraph (Csardi and Nepusz, 2006). Within each network, each node is a CDRH3 and links between nodes were drawn if the inter-node Levenshtein distance is maximally 1 aa. Degree distributions of each repertoire were also determined using the igraph degree ()-function. The degree of a node is the number of nodes it has links to (=number of CDRH3s 1 amino acid change apart).

Somatic hypermutations (SHM)

Amino acid somatic hypermutations were quantified using the the MiXCR software package v.3.04 (Greiff et al., 2017).

IEC isolation, RNA extraction and Microarray transcriptomic analysis

IECs were isolated by using a previously described method (Romagnani et al., 2017). Total RNA was extracted from IECs through Trizol precipitation (Thermo Fisher) and then digested with DNase I at 37 °C for 15 min to remove any contaminating DNA. The quality of total RNA was first assessed using an Agilent Bioanalyzer 2100 (Agilent Technologies, Palo Alto, CA). Biotin-labelled cDNA targets were synthesized starting from 150 ng of total RNA. Double stranded cDNA synthesis and related cRNA was performed with GeneChip® WT Plus Kit (Affymetrix, Santa Clara, CA). With the same kit was synthesized the sense strand cDNA before to be fragmented and labelled. All steps of the labelling protocol were performed as suggested by Affymetrix, starting from 5.5 μg of ssDNA. Each eukaryotic GeneChip® probe array contains probe sets for several *B. subtilis* genes that are absent in the samples analysed (*lys*, *phe*, *thr*, and *dap*). This Poly-A RNA Control Kit contains *in vitro* synthesized, polyadenylated transcripts for these *B. subtilis* genes that are pre-mixed at staggered concentrations to allow GeneChip® probe array users to assess the overall success of the assay. Poly-A RNA Controls final concentration in each target are *lys* 1:100,000, *phe* 1:50,000, *thr* 1:25,000 and *dap* 1:6,667. Hybridization was performed using the GeneChip® Hybridization, Wash and Stain Kit. It contains mix for target dilution, DMSO at a final concentration of 7% and pre- mixed biotin-labelled control oligo B2 and *bioB*, *bioC*, *bioD* and *cre* controls (Affymetrix cat #900299) at a final concentration of 50 pM, 1.5 pM, 5 pM, 25 pM and 100 pM, respectively. Fragmented and labelled sscDNA were diluted in hybridization buffer at a concentration of 23 ng/μl for a total of 2.3 μg and denatured at 99°C for 5 min incubated at 45°C for 5 min and centrifuged at maximum speed for 1 min prior to introduction into the GeneChip® cartridge. A single GeneChip® Mouse Clariom S was then hybridized with each biotin-labelled sense target. Hybridizations were performed for 16 h at 45°C in a rotisserie oven. GeneChip cartridges were washed and stained with GeneChip® Hybridization Wash and Stain Kit in the Affymetrix Fluidics Station 450 following the FS450_0007 standard protocol. The GeneChip arrays were scanned using an Affymetrix GeneChip® Scanner 3000 7G using default parameters. Affymetrix GeneChip® Command Console software (AGCC) was used to acquire GeneChip® images and generate .DAT and .CEL files, which were used for subsequent analysis with proprietary software. Raw data was

normalized using the quantile normalization of robust multiarray average (RMA) method. The identification of the differentially expressed transcripts and the hierarchical cluster analysis with Euclidean distance was performed using the commercial software Partek Genomics Suite (v6.6).

Gene Ontology (GO) enrichment analysis

The list of differentially expressed genes were loaded into DAVID Bioinformatics Resources (v6.8) (https://david.ncifcrf.gov) (Huang da et al., 2009) for GO enrichment analysis and visualized using the R package *GOplot* (Walter et al., 2015) and *ggplot* (Wickham et al., 2019).

Metabolomics analysis of portal vein serum and data analysis

Portal vein serum samples from C57BL/6 and *Igh-J*$^{-/-}$ monocolonized mice were collected and stored at -80°C until analysis. A targeted metabolomic assay was performed by using the Biocrates AbsoluteIDQ® p180 Kit (Biocrates life Sciences AG, Innsbruck, Austria).

Briefly, the flow injection analysis tandem mass spectrometry (MS/MS) method was used to quantify 180 known small molecule metabolites simultaneously by multiple reaction monitoring using an Acquity UPLC chromatographic system (Waters, Millford, MA, USA) coupled with a Xevo TQ-MS mass spectrometer (Waters, Millford, MA, USA). Quantification of metabolites was achieved by reference to appropriate internal standards. Reproducibility of the assay was performed on QC serum samples. Metabolomic data analysis was limited to the 139 compounds reliably detected on the samples. Missing values were imputed by a random number between zero and the metabolite specific limit of detection. All the statistical analyses were performed on the log transformed intensities to compensate for the known non-normal distribution of metabolomics data. All the analyses were performed in R (Team, 2017) relying on tidyverse and ggplot (Wickham et al., 2019) for data visualization and manipulation. The class specific metabolic dispersion was evaluated on the euclidean distance matrix in terms of beta-diversity applying the Marti Anderson's PERMDISP2 procedure for the analysis of multivariate homogeneity of group dispersions (variances). In presence of comparable dispersions, the significance of the difference between the groups was tested by permanova. Both approaches are available in R through the vegan R package (Oksanen et al., 2020). Due to the limited number of samples, pairwise comparisons were performed by univariate t-test. Due to the expected correlation between the metabolites, p-values were not corrected for multiplicity.

Two-photon imaging

E-cadherin^{mCFP} SPF mice were colonized with GFP expressing *E. coli*^{pAPyr} or *E. coli*^{pBAD28} (see mice and *in vivo* experiments method section) before euthanization and two-photon analysis. Proximal colon portions were immediately collected after sacrifice and cleaned from abdominal fat and connective tissue. Samples were then acquired without opening. Images were acquired with a Trimscope II upright two-photon microscope (LaVision Biotec) with a Nikon 25x water immersion objective (Nikon MRD77220 25x/NA 1.10). For optimal sampling, pixel size in the axial direction was 186 nm and z-step size 1 μm. Ti:Sa lasers were tuned at 925 nm and 830 nm, and emission fluorescence was collected in the ranges 450-495 nm (CFP), 500-550 nm (GFP), 590-635 nm (autofluorescence) and separated with dichroic mirrors at 560 nm, 495 nm, 635 nm. Beam diameter was set to slight overfill for improving resolution. Images were analysed with Fiji/ImageJ and spectral unmixing plugin. Images were first combined into stacks, then an unmixing matrix was applied to separate CFP, GFP and autofluorescence signals. Stacks were then resliced without interpolation in XZ planes. Finally, the distance from the epithelium was measured for each bacterium.

Sampling, fixation and histochemical staining for mucus layer thickness measurement

Proximal colon segments were fixed in Carnoy's fixative over-night then incubated 1 h in 70% ethanol, 1 h in 80% ethanol, 1 h in 96% ethanol, 3.15 h in 100% ethanol, 3.5 h in xylene and 3 h in paraffin. Serial cross sections of formalin-fixed, paraffin-embedded murine colon tissues were stained with haematoxylin and eosin as well as with a combined alcian blue and periodic acid-Schiff (PAS) staining. For the latter, sections were deparaffinized and rehydrated before staining in 1% Alcian blue solution pH 2.5 (1 g Alcian blue in 100 ml 3% acetic acid) for 30 min in a water bath at 60°C. Thereafter, sections were rinsed in tap water and stained in 0.5% periodic acid for 10 min, followed by 10 min in Schiff's reagent and 6 min in 0.52% sodium bisulphite. Sections were then stained in Weigert's haematoxylin, consisting of ferric chloride solution and 1% haematoxylin in absolute alcohol in equal amounts, for 5 min. After rinsing again in running tap water, sections were differentiated by hydrochloric acid-ethanol followed by dehydration and mounting.

Bacterial taxonomic profiling by 16S rRNA amplicon sequence analysis

Extraction, lysis and DNA isolation was done by using the Fast DNA Stool Mini Kit (Qiagen) according to manufacturer's recommendation. Bead beating was run on a fastprep24 instrument (MPBiomedicals; 4 cycles of 45 s at speed 4 followed) in 2 ml screwcap tubes containing 0.6 g 0.1 mm glass beads. 200 μl of raw extract was prepared for DNA-isolation. Concentration of the isolated DNA was assessed with PicoGreen measurement (Quant-iTT PicoGreenT dsDNA Assay Kit, Thermo Fisher) and integrity was checked by agarose gel electrophoresis for a random sample. For the amplification of the bacterial 16S rRNA gene, a primer set specific for the V3–V4 hypervariable regions was used (Fw: 5′- CCT ACG GGN GGC WGC AG -3′ (SEQ ID NO: 4); and Rev: 5′-GAC TAC HVG GGT ATC TAA TCC -3′ (SEQ ID NO: 5)). Subsequently, the Illumina MiSeq platform and a v2 500 cycles kit were used to sequence the PCR libraries. The produced paired-end reads, which passed Illumina's chastity filter, were subjected to

de-multiplexing and trimming of Illumina adaptor residuals using Illumina's real time analysis software included in the MiSeq reporter software v2.6 (no further refinement or selection). The quality of the reads was checked with the software FastQC version 0.11.8. The sequences were analyzed through the Qiime2 virtual environment (Bolyen et al., 2019). The raw sequences were in total 4'896'770 (median = 71'942, mean = 72'011.3, SD = 15'891.2). The trimming step on the first 7 and the last 25 bases and the reads filtration have allowed to obtain excellent quality sequences (Phred > 30). A denoising algorithm (Callahan et al., 2016) was implemented on these sequences. The overlapping regions R1 and R2 were joined and the chimeric reads discarded. The reads that resulted from trimming, filtering and joining steps were in total 1'145'671 (median = 16'277, mean= 16'848.1, SD= 3'897.6). The taxonomic assignment was performed by BLAST feature-classifier. It performs BLAST+ local alignment between query and reference reads. Then, it assigns consensus taxonomy to each query sequence on the last database version of Greengenes (gg_12_10). A rooted tree was constructed based on IQ-TREE stochastic algorithm that allows maximum likelihood analysis of large phylogenetic data (Nguyen et al., 2015). Sequence reads from 16S rRNA gene profiling have been deposited in the European Nucleotide Archive (ENA) of the European Bioinformatics Institute under the accession number of the study: PRJEB49686.

QUANTIFICATION AND STATISTICAL ANALYSIS

All statistical analyses were performed using the statistical programming environment R version 4.0.3 (Team, 2017) or GraphPad Prism v7.04 (GraphPad Software, La Jolla, CA, USA). Alpha diversity was calculated using the main indexes to allow an exploration of data in term of richness and evenness. Alpha-diversity estimates were computed using the phyloseq R package (McMurdie and Holmes, 2013). Statistically significant changes in the alpha diversity were determined through the Mann-Whitney signed-rank test. The microbial community comparison was calculated using PERMANOVA on Weighted distance metrics performed by UniFrac algorithm (Lozupone et al., 2011). Statistically significant differences in the relative abundance of ASVs between groups were performed by Wald test using FDR p value correction following DESeq2 read counts normalization. Statistical significance was set at $p \leq 0.05$ (*, $0.01 \leq p \leq 0.05$; **, $0.001 \leq p \leq 0.01$; ***, $p \leq 0.001$). the mean differences with $0.05 < p \leq 0.10$ were accepted as trends.